ANNUAL REVIEWS

Annual Review of Earth and Planetary Sciences

Fluids of the Lower Crust: Deep Is Different

Craig E. Manning

Department of Earth, Planetary and Space Science, University of California, Los Angeles, California 90095-1567, USA; email: manning@epss.ucla.edu

Annu. Rev. Earth Planet. Sci. 2018. 46:67–97

First published as a Review in Advance on March 12, 2018

The *Annual Review of Earth and Planetary Sciences* is online at earth.annualreviews.org

https://doi.org/10.1146/annurev-earth-060614-105224

Keywords

fluids, lower crust, metamorphism, conductivity

Abstract

Deep fluids are important for the evolution and properties of the lower continental and arc crust in tectonically active settings. They comprise four components: H_2O, nonpolar gases, salts, and rock-derived solutes. Contrasting behavior of H_2O-gas and H_2O-salt mixtures yields immiscibility and potential separation of phases with different chemical properties. Equilibrium thermodynamic modeling of fluid-rock interaction using simple ionic species known from shallow-crustal systems yields solutions too dilute to be consistent with experiments and resistivity surveys, especially if CO_2 is added. Therefore, additional species must be present, and H_2O-salt solutions likely explain much of the evidence for fluid action in high-pressure settings. At low salinity, H_2O-rich fluids are powerful solvents for aluminosilicate rock components that are dissolved as polymerized clusters. Addition of salts changes solubility patterns, but aluminosilicate contents may remain high. Fluids with $X_{salt} = 0.05$ to 0.4 in equilibrium with model crustal rocks have bulk conductivities of $10^{-1.5}$ to 100 S/m at porosity of 0.001. Such fluids are consistent with observed conductivity anomalies and are capable of the mass transfer seen in metamorphic rocks exhumed from the lower crust.

1. INTRODUCTION

Fluids play an important role in the evolution and properties of the deep continental crust. Although much is understood about their occurrence, chemistry, and flow at shallow depths, less is known about fluids in deeper crustal settings. In the absence of constraints, assumptions about lower-crustal fluids and their solutes have often been based on behavior at more familiar low-pressure conditions. However, recent progress reveals that deep fluids differ fundamentally from their shallow counterparts.

Evidence for the presence of fluids in the lower part of tectonically active continental and arc crust comes from the rock record and geophysical observations. Rocks exhumed from depths greater than ~15 km commonly contain evidence for the participation of a fluid phase in metamorphism and magmatism (Ague 2014, Etheridge et al. 1983, Ferry 1994). Rocks being transported from the surface into the deeper crust are subjected to increasing temperature (T) and pressure (P). The mineral assemblages that evolve during tectonic burial contain progressively lower volatile contents at thermodynamic equilibrium. For example, model basalt, pelite (fine-grained clay-rich sediment), and ultramafic rock, which may initially contain 5–10 wt% H_2O due to weathering, alteration, or primary mineral constituents at Earth surface conditions, contain <1 wt% H_2O at lower-crustal metamorphic grades; other volatiles follow suit (e.g., Ague 2014, Fyfe et al. 1978, Shaw 1956, Yardley et al. 1991). Direct evidence that these constituents are present in a free, lower-crustal fluid phase comes from fluid inclusions trapped in the metamorphic minerals in rocks exhumed from this environment (Crawford & Hollister 1986, Touret 2001, Yardley & Bodnar 2014). Metasomatic changes in rock compositions also provide evidence of interaction with fluids during metamorphism (e.g., Ague 1991, 1994a,b; Dipple & Ferry 1992; Yardley & Bottrell 1992). Metamorphic veins are fractures that are in many cases filled by minerals precipitated from fluids, and they often record strong chemical interaction between the fluid and the surrounding rock. Isotopic studies reveal fluid passage, in some cases in large volumes (Ferry 1994). Finally, where metamorphism is attended by magmatism, as in volcanic arcs, the crystallization of magmas in the deep crust leads to input of externally derived magmatic fluids into deep-crustal metamorphic systems (e.g., Annen et al. 2006, Cashman et al. 2017).

Evidence from the rock record indicates chemical interactions in the geologic past, whereas geophysical data can show where they are occurring today. Magnetotelluric results from a range of tectonically active settings reveal the presence of deep-crustal conductive zones that have been interpreted to indicate the presence of a free fluid phase (Hyndman & Shearer 1989, Shankland & Ander 1983). Examples include areas of continental collision such as Tibet and New Zealand (Bai et al. 2010, Chen et al. 1996, Li et al. 2003, Wannamaker et al. 2002, Wei et al. 2001), immature to mature continental crust above subducting oceanic crust (Evans et al. 2014, Ichiki et al. 2009, McGary et al. 2014, Mishina 2009, Ogawa et al. 2001, Wannamaker et al. 2014, Worzewski et al. 2011, and references therein), transform plate boundaries (Becken & Ritter 2012), and continental rifts (Meqbel et al. 2014). In each case, conductive anomalies are identified at depths greater than about 15 km but above the Moho. In areas of active magmatism, as in Tibet or continental arcs, magmas may explain some of this signal; however, the high magmatic H_2O contents that elevate magmatic conductivity (Laumonier et al. 2017) also lead to deep saturation with a fluid phase, so that both phases may contribute to observed conductivity. Regardless, many observations of elevated conductivity are from regions where T is subsolidus. Of particular note is the consistent observation in volcanic arc crust of a conductive anomaly at 20–30 km depth and some 30 km trenchward from the volcanic front (Worzewski et al. 2011). Thermal models predict temperatures in this region that are below wet crustal melting, so the presence of a conductive pore fluid is the best explanation. The conductive anomalies extend below the Moho to the subducting slab. It is

commonly assumed that such anomalies trace the path of fluids derived from the basalt-eclogite transformation in the slab; however, it is worth noting that within the crust this region is also likely undergoing active metamorphism, with attendant production of a fluid phase as devolatilization reactions proceed.

Seismic data support the inference that fluids are present in tectonically active lower crust based on resistivity. Slow earthquake phenomena such as episodic tremor and low-frequency earthquakes (Beroza & Ide 2011) may be spatially correlated with crustal zones of low resistivity in convergent margins (Aso et al. 2013, Kao et al. 2005) and the San Andreas fault (Shelly & Hardebeck 2010). Similar correlations are observed in seismic velocity and attenuation and small-earthquake distribution (Reyners & Eberhart-Phillips 2009). Fluids transmitted from the deep crust may also play a role in the generation of major earthquakes at the base of the seismogenic zone, such as the 1995 M7.2 Kobe earthquake at 18 km depth (Zhao et al. 1996, 2002).

The compositions and properties of deep fluids are in part controlled by the host rocks in which they are confined, so interpretations of metasomatism, resistivity structure, or seismicity require consideration of the chemical consequences of fluid-rock interactions. In this review, I highlight recent advances that are leading to new understanding of these interactions in the lower crust. Recent reviews of crustal fluids provide general background (Ague 2014, Yardley & Bodnar 2014); here the focus is on the chemical properties of these fluids and the solutes they carry in the context of interactions with the mineral matrix that hosts them.

The term "crust" refers to continental, nonoceanic crust, regardless of maturity—a distinction that allows consideration of processes affecting settings ranging from juvenile volcanic arcs to more mature continents. In addition, the attention here is on crust undergoing active tectonism, magmatism, and metamorphism. Stable continental interiors are not considered, though at least local presence of deep-crustal fluids has been proposed (e.g., Hyndman & Shearer 1989), leading to vigorous debate (Frost & Bucher 1994, Wannamaker 2000, Yardley & Valley 1997).

The deep crust is chemically and seismically distinct from the shallow crust, but there is no distinct boundary (e.g., Rudnick & Gao 2003). Here I generally follow Holbrook et al. (1992) in defining the deep crust as the region between the Conrad discontinuity and the Moho (i.e., their middle and lower crust). Most generally, I am interested in the crust below the brittle-ductile transition, where low rock strength and plastic deformation yield a fundamentally different hydrologic regime (Ague 2014, Connolly 2010, Manning & Ingebritsen 1999). Based on the settings in which deep fluids are inferred, I examine the properties of fluids at a range of P and T. The focus is on pressures of 0.5–1.5 GPa, the interval that approximates depths from ~15–60 km for a reasonable spread of crustal densities. A wide range of temperatures may obtain within the lower crust (e.g., Artemieva & Mooney 2001), from 300°C or less in nonmagmatic settings to >800°C, well above the temperature of H_2O-saturated melting of most crustal lithologies. Higher pressures are attained during ultrahigh-P metamorphism in the deepest parts of continent-continent convergence zones, but here I limit attention to the more pedestrian depths where geophysical, petrologic, and geochemical data are converging to reveal an important role for fluids.

2. BULK PROPERTIES OF DEEP-CRUSTAL FLUIDS

Deep fluids are complex mixtures of four essential ingredients (**Figure 1**): H_2O, gases (chiefly CO_2), salts (chiefly alkali chlorides), and host-rock oxide components (chiefly silicates and aluminosilicates). I begin by examining properties of $H_2O \pm$ gas $\pm$ salt solutions, which generally determine a deep fluid's solvent properties (**Figure 1**). The chemical and physical interactions between this solvent and its host rock yield modified fluid composition and properties, so I turn in Section 3 to interactions between deep fluids and rock-forming minerals.

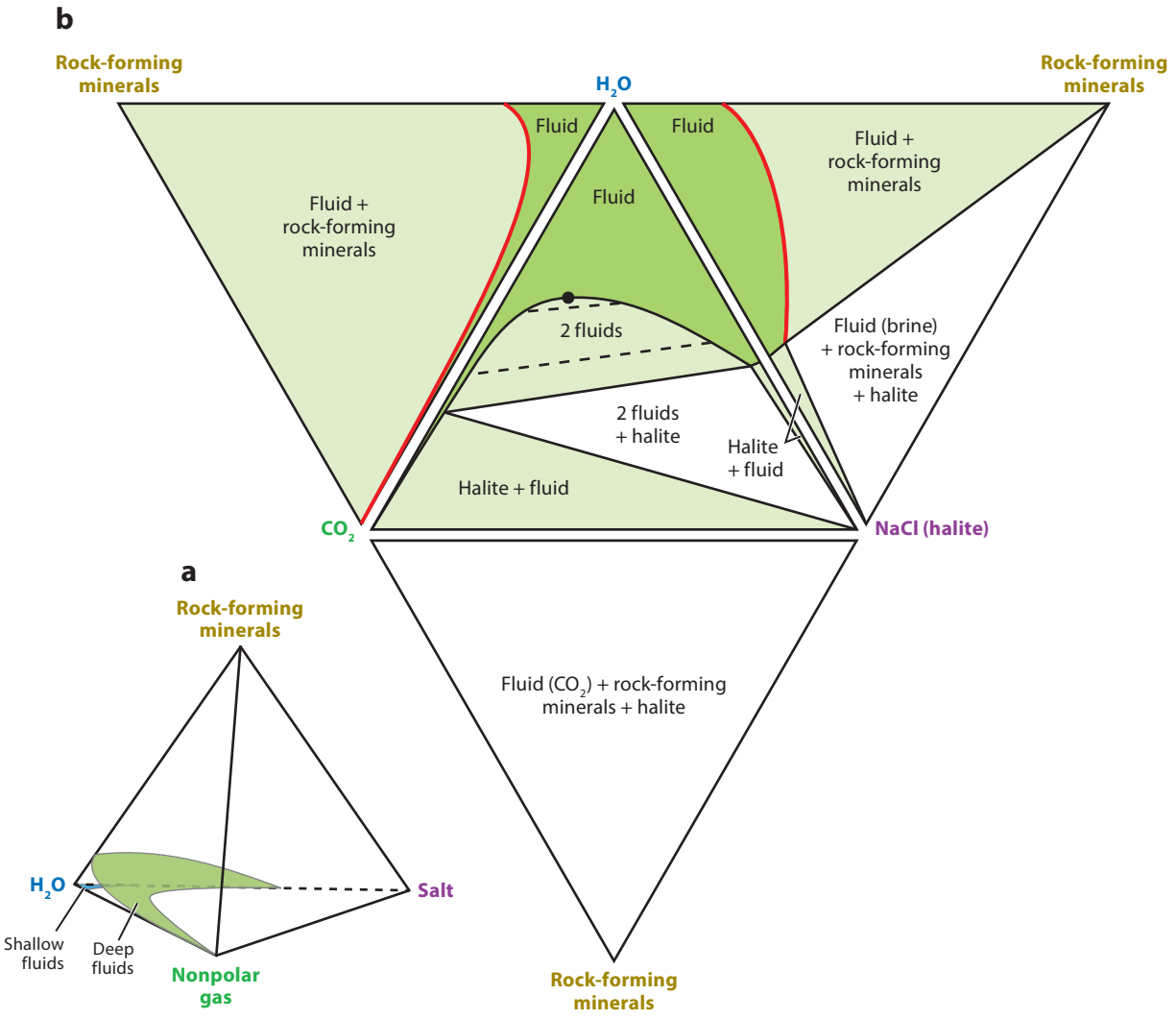

Figure 1

(*a*) The deep-fluid tetrahedron. Deep fluids comprise four components: H_2O, nonpolar gases, salts, and other material derived from dissolution of rock-forming minerals. Shallow fluids are H_2O rich, possessing very low solubility of gases and minerals; modest salinities up to salt saturation may be attained. Consequently, shallow fluids in equilibrium with rock-forming minerals (*blue*) will plot very close to the H_2O apex and effectively lie on the basal face of the tetrahedron. Deep fluids have substantially higher concentrations of other constituents in addition to H_2O, owing to high salinity at salt saturation and complete mixing of H_2O and most nonpolar gases. Where equilibrated with rock-forming minerals (*green*), deep fluids will plot on a surface significantly elevated above the basal face of the tetrahedron. (*b*) Model of deep fluid at 800°C and 0.9 GPa, using H_2O, CO_2, and NaCl as solvent components. Panel modified from Manning et al. (2013). One-, two-, and three-phase fields are shown in dark green, light green, and white, respectively. The central triangle shows phase relations in the fluid in the absence of any solutes other than NaCl and CO_2. A single H_2O-CO_2-NaCl fluid is stable in the H_2O-rich region but separates into two fluids, one NaCl rich and one CO_2 rich, as H_2O concentration decreases with addition of NaCl and CO_2 (coexisting compositions are shown with dashed lines). Dissolution of rock-forming minerals adds solutes, as shown schematically in the bounding triangles. Since all deep fluids will coexist with rock-forming minerals, the most important composition is that at rock-forming mineral saturation (*red lines*). The topology of the red lines varies with mineral assemblage, *P*, and *T*, but there are no deep-crustal conditions at which there is significant solubility of rock-forming minerals in CO_2 ± halite.

As in the shallow crust, the most important component of deep fluids is H_2O. Its polar geometry and unique intermolecular interactions make it an especially powerful and mobile solvent at lower-crustal conditions. Although the microscopic structure of H_2O remains poorly known at high P, a key difference relative to liquid water at ambient conditions is the distortion and diminishing number of intermolecular hydrogen bonds with increasing P and T (Foustoukos & Mysen 2012, Frantz et al. 1993, Sahle et al. 2013, Walrafen et al. 1996, Yoshii et al. 2001).

Nonpolar gas components may also be abundant in deep-crustal fluids. The most common example is CO_2. At oxygen fugacity (fO_2) corresponding to quartz-fayalite-magnetite equilibrium or higher, oxidized forms such as CO_2 predominate; however, CH_4 may become prevalent (along with H_2) at lower fO_2. CO and hydrocarbons typically occur only as minute constituents. Other gases, including N_2, are present in subordinate to trace concentrations.

The prevalence of CO_2 as the main nonpolar gas constituent led early workers to model deep-crustal fluids as simple mixtures of H_2O and CO_2, or more complex mixtures of C–O–H gas species. Most data came from the investigation of very-high-grade metamorphic rocks—granulites—which require T in excess of ~700°C and activity of H_2O (a_{H_2O}) substantially less than one. Assuming the presence of a free fluid phase, the favored mechanism to reduce a_{H_2O} was addition of CO_2 (e.g., Newton 1980, Newton et al. 1980), based in part on observations of fluid inclusions rich in this component. However, late relative ages of some inclusions and phase equilibrium arguments raised serious problems for this model (e.g., Lamb & Valley 1987, 1988) and led many to conclude that only crustal melting could explain the observations. However, terranes recording the transition to granulite-facies metamorphism indicate that a_{H_2O} is commonly in the range 0.3–0.5 (Newton et al. 2014), higher than is consistent with a melt but still requiring an additional fluid component.

The problem of reduced H_2O activity in a free lower-crustal fluid is at least in part resolved by high concentrations of halogens. Direct evidence for saline deep fluids comes from the rock record in the form of rare halide minerals, fluid inclusions, and high Cl contents of key high-grade metamorphic minerals (Markl & Bucher 1998, Newton et al. 1998, Touret 1985, Trommsdorff et al. 1985). Chlorine typically predominates (Yardley & Graham 2002), and the halogen anions are accompanied by charge-balancing metal cations, most commonly alkalis—hence the common reference to NaCl- and/or KCl-rich saline fluids or brines. It is important to note, however, that at deep-crustal conditions these components exist in solution largely as dissociated ions, such as Na^+ and Cl^- (Aranovich & Newton 1996, 1997).

In the shallow crust, strongly nonlinear physical chemical properties arising from critical phenomena in H_2O and CO_2 can dominate the thermodynamic, transport, and solvent behavior of fluids. In the deep crust, conditions are far removed from the one-component critical points of H_2O, CO_2, and other pure fluids. This leads to smooth variations in properties of pure fluids, and complete mixing in binary solutions of H_2O with most other constituents (H_2 is an exception; Bali et al. 2013). However, as reviewed by Manning & Aranovich (2014), in the deep crust the properties of mixtures of water and nonpolar gases differ greatly from those of water-salt mixtures. H_2O activity in H_2O-NaCl and H_2O-KCl fluids shows negative departures from ideal molecular mixing, consistent with nearly ideal, fully dissociated molten salt behavior at lower-crustal conditions (Aranovich & Newton 1996, 1997). In contrast, a_{H_2O} in mixtures with nonpolar gases is greater than in ideal mixtures (Ferry & Baumgartner 1987, Manning & Aranovich 2014, and references therein). This has important consequences for water-gas-salt mixtures, for example, H_2O-CO_2-NaCl. The contrasting mixing properties along the respective binaries, coupled with minute mutual solubilities of CO_2 and NaCl liquid, lead to an extensive region of immiscibility in the ternary at deep-crustal conditions (**Figure 1*b***) (see Aranovich et al. 2010, Heinrich 2007, Liebscher 2010, and references

therein). The immiscibility persists in the presence of other components; for examples and reviews of general phase equilibria see Fyfe et al. (1978), Heinrich (2007), and Yardley & Bodnar (2014).

Variations in composition, *P*, and *T* cause changes in the fluid properties that govern interactions with host rocks, including density, dielectric constant, self-dissociation behavior, and conductivity. In view of the immiscibility described above, these are discussed below by starting with H_2O and then considering H_2O-CO_2 and H_2O-NaCl solutions as models.

2.1. Density

Knowledge of the *P-V-T* properties of H_2O has long been limited by challenges associated with experimental work at high *P* and *T*. However, advances in diamond-cell technology and computer simulation have produced new constraints that lend improved accuracy (e.g., Abramson & Brown 2004; Pan et al. 2013, 2014; Sanchez-Valle et al. 2013). **Figure 2*a*** illustrates the variation in H_2O density with temperature at a range of depths and along simple linear geotherms of 10°C/km, 20°C/km, and 40°C/km, which model d*P*/d*T* associated with burial/exhumation and heating/cooling in a range of settings. The density of liquid H_2O at ambient conditions is ~1 g/cm^3. Increasing temperature with depth at shallow-crustal conditions can yield decreases in density well in excess of 50%. However, at deep-crustal conditions ranging from 0.5 to 1.5 GPa, H_2O density lies in a relatively narrow range of 0.6 to 1.2 g/cm^3, and for a wide range of settings will be within ~10% of 1 g/cm^3 (**Figure 2*a***). This is emphasized by 10°C/km and 20°C/km geothermal gradients, which exhibit relatively little change over the interval of interest. The modest density changes arise from the low compressibility and expansivity of H_2O at depth, which in turn derive from the strong interactions between H_2O molecules in the fluid.

The low molecular weight of H_2O means that addition of most other components, such as CO_2 and alkali halides, will increase fluid density. The contrasting mixing properties of CO_2 and NaCl with H_2O yield different compressibility behavior within the lower crust. **Figure 2*c*** shows that, relative to volume at 0.5 GPa and 700°C, a fluid with CO_2 mole fraction (X) of 0.5 is more compressible than pure H_2O, because of the diminishing consequences of the positive volume of mixing between these two species. In contrast, H_2O with 5 molal (22 wt%) NaCl is less compressible than pure H_2O, consistent with strong disruption of H_2O structure by NaCl at all *P* shown. In general, addition of nonpolar gases or alkali halides changes fluid compressibility behavior only by a few percent over the pressure interval of the lower crust. Recent modeling, first-principles simulations, and high-quality experimental results are providing new insights into key related properties relevant to geophysical study of mixed fluids in the lower crust (Mantegazzi et al. 2013, Mao et al. 2015, Sakuma & Ichiki 2016a, Sakuma et al. 2013, Sanchez-Valle et al. 2013).

2.2. Dielectric Constant

The dielectric constant is the ratio of a material's permittivity to that of a vacuum, and along with density it contributes to the solvent properties of H_2O and more complex, mixed fluids. The higher the dielectric constant, the more effectively solvent molecules shield oppositely charged ions from the coulombic attractions that lead to ion pairing and mineral precipitation.

Until recently, a lack of experimental constraints on the dielectric constant of H_2O at lower-crustal conditions (≥0.5 GPa) has been a major limitation in studying water-rock interaction in this setting. The numerous formulations yielding high *P-T* estimates agree well at low *P* where constrained by experiment but yield strongly varying extrapolated values at lower-crustal conditions. A significant recent advance has been new first-principles molecular dynamics simulations (Pan et al. 2013), which yield robust constraints at high *P* and *T*. This has led to a new formulation

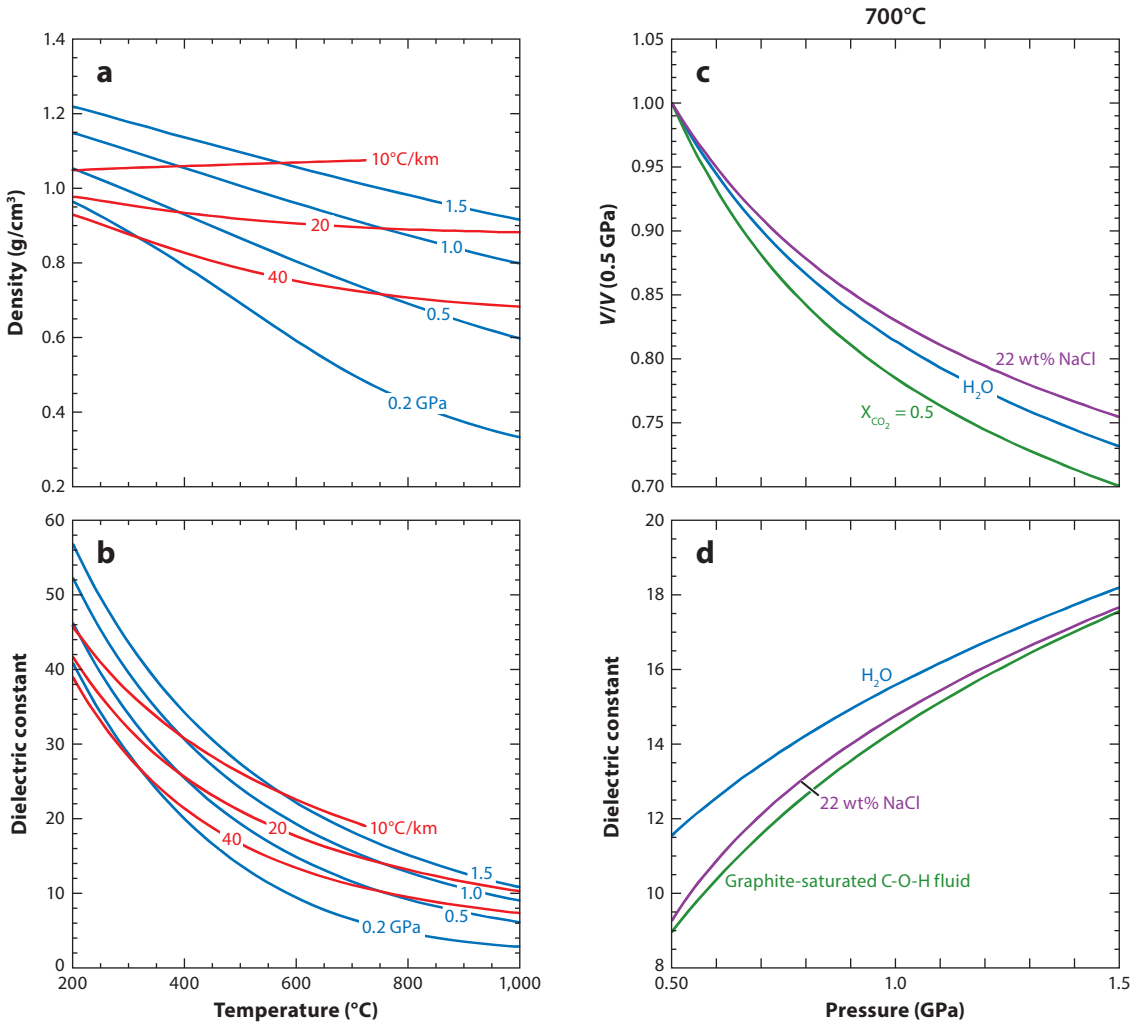

Figure 2

Variation in (*a*) the density and (*b*) the dielectric constant of H_2O with temperature along 0.2, 0.5, 1.0, and 1.5 GPa isobars (*blue*) and along linear geothermal gradients of 10°C/km, 20°C/km, and 40°C/km (*red*). Densities were calculated using Zhang & Duan (2005); dielectric constants are from Sverjensky et al. (2014). (*c*) Relative decrease in volume of H_2O and mixed fluids with pressure from 0.50 to 1.5 GPa at 700°C. Data are from Duan & Zhang (2006) and Sakuma & Ichiki (2016a). (*d*) Variation in dielectric constant of mixed fluids with pressure at 700°C (Foustoukos 2016, Galvez et al. 2015). Gas species in C–O–H fluid vary with pressure at graphite saturation.

of dielectric constant to 6 GPa and 1,000°C (Sverjensky et al. 2014), which can now be used in geochemical studies of aqueous fluids and their interactions with deep-crustal rocks. Additional constraints were provided by Sakuma et al. (2013), although their values are consistently lower than those from experiments at similar conditions.

Figure 2*b* shows that the dielectric constant of H_2O in the lower crust is everywhere lower than the value of 78 characteristic of ambient conditions. Values decrease with *T* along each isobar and geotherm, while increasing slightly with isothermal increase in *P*. These patterns indicate that temperature is the primary control on dielectric constant at lower-crustal conditions. The isobaric

decline in the dielectric constant of H_2O is consistent with a decreasing extent of hydrogen bonding (Foustoukos & Mysen 2012, Yoshii et al. 2001).

Addition of components such as CO_2 and NaCl modifies the structure and solvent properties of the fluid phase, and hence the dielectric constant. There are no direct measurements of dielectric constant in mixed fluids at lower-crustal conditions, but recent developments now permit estimation at conditions relevant to the deep crust. Galvez et al. (2015) used the approach of Harvey & Prausnitz (1987) to derive the dielectric constant of mixed C–O–H fluids. **Figure 2*d*** shows variation in the dielectric constant at 700°C and 0.5 to 1.5 GPa for a graphite-saturated C–O–H fluid. The relative abundance of specific gas species in the fluid varies with pressure. The dielectric constant of the fluid mixture is about 22% lower than that of pure H_2O at 0.5 GPa, but only 4% lower at 1.5 GPa. Mountain & Harvey (2015) noted that the Harvey & Prausnitz (1987) method may overestimate dielectric constant in mixtures of nonpolar gases. For example, at 1,000 K and 1 GPa, their molecular dynamics calculations yield a dielectric constant of 2.8 for a fluid with $X_{CO_2} = 0.5$, as compared to 3.2 using the Harvey & Prausnitz model.

Foustoukos (2016) extended this approach to H_2O-NaCl, using a simple empirical model based on the solubility of quartz in H_2O-NaCl brines (Newton & Manning 2000). Results indicate that, for a 22 wt% NaCl solution (5 molal), the dielectric constant of the mixed fluid is similar to that in a graphite-saturated C–O–H fluid (**Figure 2*d***).

2.3. H_2O Self-Dissociation

Another key property of H_2O at deep-crustal conditions is that it exhibits a substantially greater tendency to dissociate to its constituent ions (Marshall & Franck 1981). That is, at equilibrium, the reaction

$$H_2O = H^+ + OH^- \qquad 1.$$

proceeds further to the right than at more familiar ambient and upper-crustal conditions, indicated by greater values of the equilibrium constant K of Equation 1:

$$K_1 = \frac{a_{H^+} a_{OH^-}}{a_{H_2O}}, \qquad 2.$$

where a is activity of the subscripted species. Deep-crustal values of K_1 range from $\sim 10^{-10}$ to $\sim 10^{-7}$, as opposed to $\sim 10^{-14}$ at ambient conditions. Although the equilibrium constant is 4–7 orders of magnitude greater in the deep crust, it is not so great that molecular H_2O becomes subordinate, as in an ionic fluid at extreme P and T.

Neutral pH corresponds to the condition when H^+ activity is equal to OH^- activity. It is useful for assessing the relative acidity or alkalinity of a fluid. From Equation 2, neutral pH (pH_n) is

$$pH_n = -\frac{1}{2}\left(\log K_1 + \log a_{H_2O}\right). \qquad 3.$$

Figure 3*a* shows variation in pH_n in pure H_2O ($a_{H_2O} = 1$) in the lower crust. Neutral pH ranges from ~3.5 to 5, substantially lower than the more familiar value of 7 at ambient pressure and temperature. Neutral pH decreases with increasing T (burial) along geotherms. Thus, self-dissociation of water becomes more extensive with increasing depth. The opposite will hold for cooling and decompression paths.

The lower values of pH_n at lower-crustal conditions are important for chemical processes of water-rock interaction and for interpreting geophysical data. Low pH_n signals that, in contrast to those in shallow-crustal environments, the concentrations of the H_2O self-dissociation products

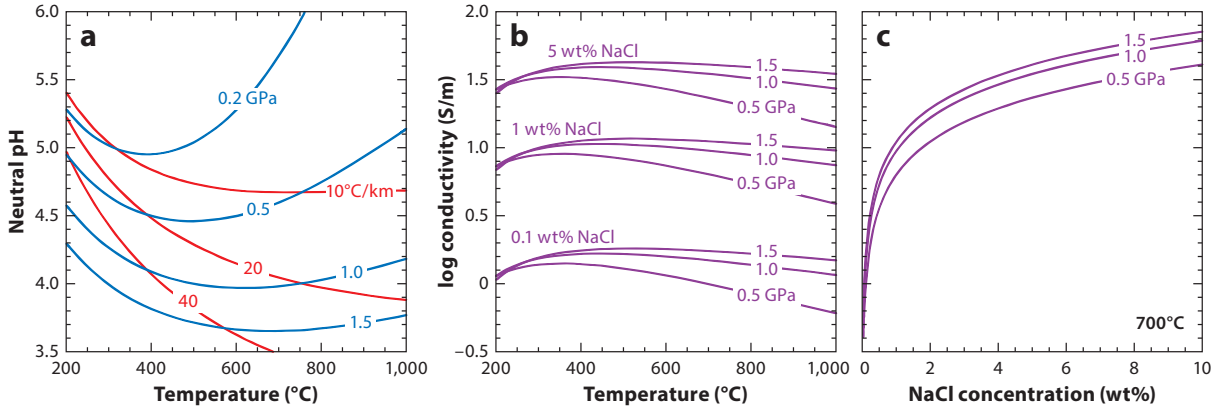

Figure 3

(*a*) Variation in neutral pH in H_2O with temperature along 0.2, 0.5, 1.0, and 1.5 GPa isobars (*blue*) and along linear geothermal gradients of 10°C/km, 20°C/km, and 40°C/km (*red*). Curves were calculated using values of K_1 from Sverjensky et al. (2014). (*b*) Isobaric variations in conductivity with temperature of 0.1, 1, and 5 wt% NaCl solutions. (*c*) Isobaric variations in conductivity with NaCl concentration at 700°C. Curves in panels *b* and *c* were calculated using equations from Sinmyo & Keppler (2017); values at >5.5 wt% in panel *c* are extrapolated.

H^+ and OH^- are quite high in the deep crust. This suppresses extremes in pH that are found near Earth's surface because, at depth, higher concentrations of other ions are required to achieve the same pH shift from neutrality. Note however that H^+ and OH^- concentrations are still sufficiently low that the ionic strength of pure H_2O is modest: For $pH_n = 3.5$, ionic strength is only $2 \times 10^{-3.5}$, where ionic strength (I) quantifies the bulk effect of charged species and is calculated as

$$I = \frac{1}{2}\sum_i m_i z_i^2. \qquad 4.$$

In Equation 4, m_i and z_i are molality and charge, respectively, of the ith solute ion. Because charge is squared, more highly charged electrolytes will have greater effects on ionic strength. In this article, I refers to true ionic strength, i.e., that arising solely from those solutes present in ionic form. Ionic strength is used in the calculation of ion activity coefficients and is linked to conductivity.

Neutral pH depends on H_2O activity (Equation 3), so high concentrations of gas or salt are expected to modify acid-base neutrality relative to H_2O-rich fluids. However, even though salts and polar gases have contrasting effects on a_{H_2O}, their effect on pH_n is minor: Equation 3 shows that, even if a_{H_2O} is as low as 0.1, pH_n is increased only by 0.5.

2.4. Conductivity

While the extent of self-dissociation in deep-crustal fluids is enhanced relative to shallow fluids, pure H_2O nevertheless remains a poor conductor at these conditions. Values are in the range 0.01–1 S/m (e.g., Holzapfel 1969, Marshall & Franck 1981). Because porosity is generally low, explaining elevated bulk conductivity in the deep crust by the presence of a fluid phase requires additional dissolved, conductive components.

Conductivities of mixtures of H_2O and CO_2 (or other nonpolar gases) have not been measured but can be expected to decline significantly with increasing gas concentration due to strong reduction in dielectric constant (e.g., Mountain & Harvey 2015). This expectation may break down at

low CO_2 concentrations, where recent first-principles results suggest that carbonate and bicarbonate ions predominate over molecular CO_2 (Pan & Galli 2016), which would increase conductivity.

Experimental attention to H_2O and NaCl (or other metal halides) was long limited to upper-crustal pressures (e.g., Nesbitt 1993; Quist & Marshall 1968, 1969); however, the conductivity of H_2O-NaCl solutions at lower-crustal conditions has recently been constrained, at least to moderate salinity, by molecular dynamics and experiments (Sakuma & Ichiki 2016b, Sinmyo & Keppler 2017). **Figure 3*b*** shows conductivities calculated based on the model of Sinmyo & Keppler (2017). Results of Sakuma & Ichiki (2016b) are similar. At constant NaCl concentration, conductivity depends only modestly on P and T. However, at a given P and T, conductivity rises strongly with NaCl concentration (**Figure 3*c***). Clearly, conductivity of deep-crustal fluids depends much less on P and T than on the concentration of ionic solutes.

Foustoukos (2016) showed that the electrical conductivity of concentrated H_2O-NaCl solutions has a simple linear dependence on true ionic strength:

$$\sigma_f = cI, \qquad 5.$$

where σ_f is the fluid conductivity in S/m and $c = 79.5 \pm 0.4$ kg S mol^{-1} m^{-1}. The relation is applicable in the presence of other salts (e.g., KCl) and holds to $X_{salt} = 0.4$. The ionic strengths of such concentrated brines exceed 15 mol/kg H_2O at deep-crustal conditions, suggesting fluid conductivities >1,000 S/m.

3. SOLUTES IN H_2O

3.1. Aqueous Ions

Molecular dynamics simulations at varying levels of theory, coupled with advances in diamond-cell and synchrotron X-ray methods (e.g., Bassett et al. 1993, Chervin et al. 1995, Sanchez-Valle 2013, Schmidt & Chou 2012), are providing unprecedented insights into atomic-scale ion-water interactions at deep-crustal conditions. Molecular dynamics simulations of dilute NaCl solutions (Sakuma & Ichiki 2016a) reveal that increasing hydration numbers of Na^+ and Cl^- with P are offset by decreases with T, leading to relatively little change along a geotherm of ~20°C/km. In addition, the extent of dissociation of salt solutions increases with rising P and T (Jahn & Schmidt 2010, Pan & Galli 2016), consistent with inferences from in situ Raman spectroscopy (Frantz 1998, Frantz et al. 1994, Schmidt 2014). Recent results suggest that these general trends may break down at the lowest temperatures (Schmidt & Manning 2017).

Despite the growing capabilities of experimental and simulation approaches for characterizing the structure and energetics of ion-water interaction in simple systems, understanding of more complex fluids in equilibrium with model or natural mineral assemblages still relies on thermodynamic models of aqueous ions (Dolejš 2013). The Helgeson-Kirkham-Flowers (HKF) model is most widely used (Helgeson & Kirkham 1976, Helgeson et al. 1981, Tanger & Helgeson 1988). The HKF model provides ion properties dependent on the dielectric constant of H_2O, but lack of high-P constraints on this parameter historically limited its application to shallow-crustal conditions (≤0.5 GPa). Because H_2O density is better quantified, empirical approaches relying on density correlations (e.g., Anderson et al. 1991) have been used to explore fluid-rock interaction in deeper settings (Dolejš & Manning 2010; Manning 1998, 2013). However, new constraints on dielectric constant at high P, incorporated via the Deep Earth Water (DEW) model (Sverjensky et al. 2014), now allow extension of the HKF model to the lower crust (and beyond). The DEW model is used in this review to gain thermodynamic insight into the distribution of aqueous species in deep, water-rich fluids.

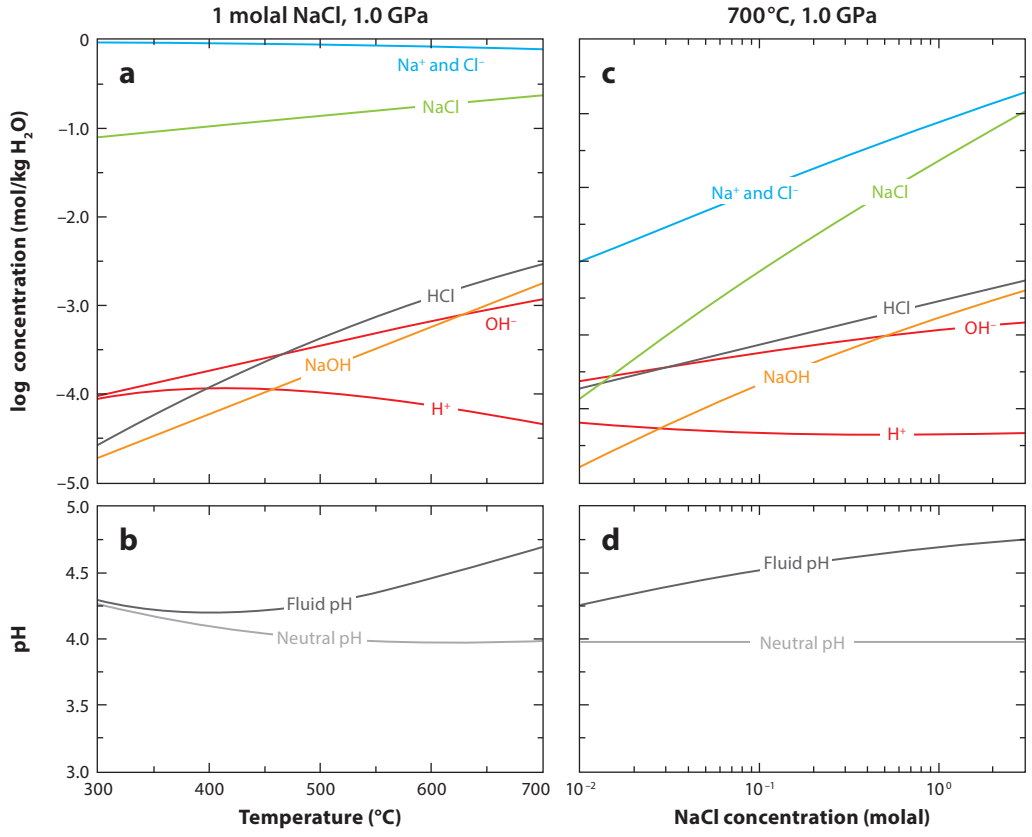

Figure 4

Isobaric variation in species concentrations and pH of NaCl solutions (*a*, *b*) with temperature (1 molal NaCl) and (*c*, *d*) with NaCl concentration (700°C). All calculations are at 1.0 GPa. Solution composition was calculated using EQ3 (Wolery 1992), thermodynamic data from the Deep Earth Water (DEW) model (version 11.0.2) of Sverjensky et al. (2014), and the b-dot model for activity coefficients.

Figure 4 illustrates the behavior of NaCl solutions at 1 GPa. For a NaCl concentration of 1 molal (**Figure 4*a*,*b***), the solution is dominated by Na^+ and Cl^- ions at all *T*. However, rising *T* produces an increasing tendency to form ion pairs in the solution, consistent with the isobaric decline in dielectric constant (**Figure 2*b***). The greater extent of ion pairing with chloride (NaCl and HCl) relative to hydroxide (NaOH) causes the pH of NaCl solutions to be alkaline, and alkalinity increases as the disparity in concentration of neutral chlorides relative to the neutral hydroxide grows with temperature. Similar effects can be seen at a given *P* and *T* as total NaCl concentration increases, e.g., at 700°C (**Figure 4*c*,*d***). Although there is an effect on pH, the overall concentration of ion pairs is low; NaCl, along with other alkali halides, remains largely dissociated as concentrations increase to salt saturation (Aranovich & Newton 1996, 1997).

3.2. Aqueous Silica and Polymerization

Ionic species are essential ingredients of all crustal fluids, deep or shallow. However, deep fluids typically differ from their shallower counterparts in that they carry a greater load of neutral solutes. This arises from higher solubility of oxide minerals coupled with elevated high-*PT* stability of

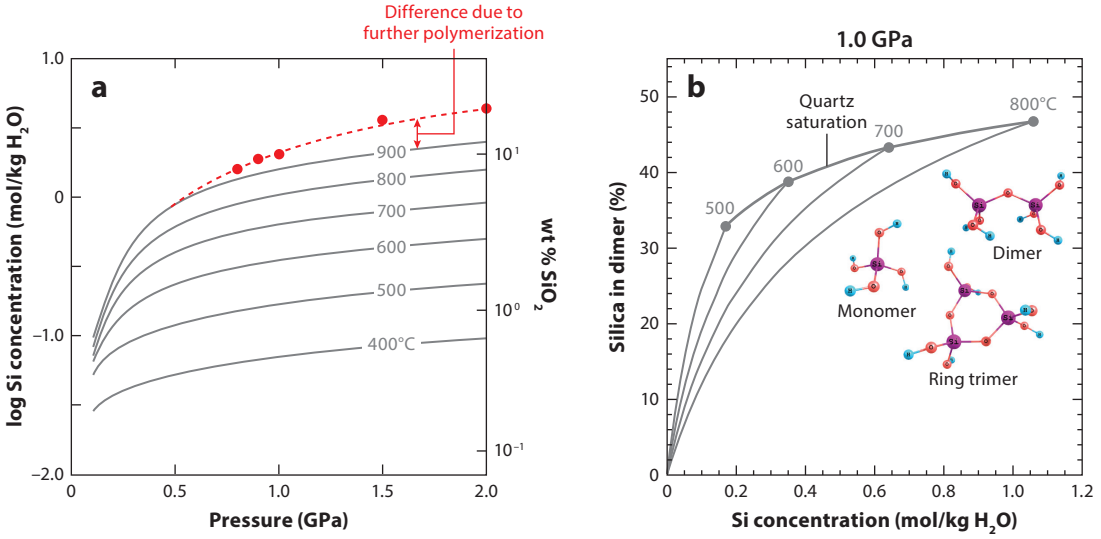

Figure 5

(*a*) Solubility of quartz as a function of pressure and temperature at lower-crustal conditions. (*b*) Variation in species abundance as a function of temperature and Si concentration at 1.0 GPa. Curves in panels *a* and *b* were calculated using unit activity coefficients and thermodynamic data from Sverjensky et al. (2014) [Deep Earth Water (DEW) model version 11.0.2)], which include only monomer and dimer forms of aqueous silica, molecular structures of which are shown in panel *b*. At high temperature (e.g., 900°C), the DEW model underpredicts quartz solubility determined experimentally (*red circles* in panel *a*) (Manning 1994, Hunt & Manning 2012), due to increasing concentration of additional species such as the ring trimer. Panel *b* shows that rising Si concentration favors increasing polymerization extent; however, the variation with temperature is at odds with bulk solubility measurements and critical mixing in the SiO_2-H_2O system.

neutral aqueous hydrates, such as H_4SiO_4. Because SiO_2 is typically the most abundant rock-forming oxide, the solubility of quartz provides a good guide to the role of *P* and *T* in mineral solubility. The increasing solubility of quartz with *P* and *T* is illustrated in **Figure 5*a***, based chiefly on experimental determinations (Anderson & Burnham 1965, Manning 1994, and references therein). Similar patterns are seen for solubilities of other simple oxides (Audétat & Keppler 2005; Becker et al. 1983; Caciagli & Manning 2003; Dolejš & Manning 2010; Tropper & Manning 2005, 2007). However, none are as high as that of quartz, which means that silica is typically one of the most abundant solute components of deep-crustal fluids.

A contribution to the high solubility of silica in H_2O is its ability to polymerize. At low concentration and neutral pH, the dominant species of dissolved silica is monomeric orthosilicic acid (H_4SiO_4). The dissolution reaction may be written as

$$\underset{\text{quartz}}{SiO_2} + 2H_2O = \underset{\text{aqueous monomer}}{H_4SiO_4}. \quad 6.$$

Equation 6 adequately describes quartz solubility in shallow settings at most conditions (e.g., Walther & Orville 1983). However, experimental phase equilibria and Raman spectroscopy at high *P* and *T* reveal the presence of silica dimers (Newton & Manning 2002b, 2003; Zhang & Frantz 2000; Zotov & Keppler 2000, 2002), which reflect combination of two monomers via sharing of a bridging oxygen (**Figure 5**), and liberation of an H_2O molecule:

$$\underset{\text{monomer}}{2H_4SiO_4} = \underset{\text{dimer}}{H_6Si_2O_7} + H_2O. \quad 7.$$

Polymerization of silica at near-ambient conditions is typically associated with high concentrations at alkaline pH (e.g., Hunt et al. 2011). Appreciation of the role played by polymerization at high *P* and *T* in near-neutral fluids has come about relatively recently.

Figure 5*b* shows the speciation of aqueous silica in H_2O at 1.0 GPa and 500–800°C. The calculations neglect deprotonated monomers ($H_3SiO_4^-$), which are negligible at these conditions. Along each isotherm, the fraction of dissolved silica in the polymerized species increases to quartz saturation. At constant pressure, rising temperature yields a decrease in the equilibrium constant for Equation 7 in the DEW model (Sverjensky et al. 2014), which translates to a decreasing extent of polymerization at a fixed Si concentration. However, this is offset by the rise in quartz solubility with temperature (Anderson & Burnham 1965, Manning 1994), leading to a progressively greater fraction of Si in dimers as temperature increases. Thus, **Figure 5*b*** shows that, at 500°C, polymerization via dimer formation accounts for ~33% extra Si solubility at quartz saturation, whereas at 800°C it accounts for ~47%.

The equilibrium constant for Equation 7 is uncertain. Values consistent with experimental results of Newton & Manning (2002b) and Zotov & Keppler (2002) imply more extensive dimer formation at any *T*, and an increase with rising *T*. The discrepancy arises from reliance of the DEW model on interpretations of Mysen (2010), which imply trends different from those observed by previous workers. Further experimental study is needed, but there is little doubt that a key feature of aqueous silica at deep-crustal conditions is its strong propensity to polymerize.

A clue to resolution of the problem is the extent of silica polymerization near hydrous melting of quartz, where solubility becomes so high that SiO_2 and H_2O can form a supercritical mixture in which the distinction between solutions and magmas is lost (Kennedy et al. 1962). Models of quartz solubility that implicitly or explicitly account for polymerization only to dimers (Gerya et al. 2005, Manning 1994, Sverjensky et al. 2014) begin to underpredict solubility as *T* rises above 800°C at high *P*. This signals the increasing abundance of more polymerized species such as the ring trimer (**Figure 5*b***) and higher oligomers (Newton & Manning 2008b). Hunt & Manning (2012) showed that a model accounting simply for the formation of individual bridging oxygens accurately predicts the melting curve and critical end point. Thus, Equation 7 is the first in a series of progressive polymerization reactions leading to the stability of supercritical SiO_2-H_2O mixtures that can range from unpolymerized to fully polymerized depending on H_2O content (e.g., Manning 2004, 2017).

3.3. Interaction Between H_2O and Deep-Crustal Rocks

Thermodynamic data for aqueous species can be used to predict the fluid that would result from equilibrium between pure H_2O and mineral assemblages for model deep-crustal lithologies. As an example, I take the mineral assemblage muscovite + K feldspar + quartz as a model for lower-crustal pelite. Other likely minerals are initially neglected to highlight key features of the predicted fluids.

Figure 6 shows model fluids as a function of *T* at 1 GPa and as a function of *P* at 650°C. The conditions portrayed are below H_2O-saturated melting (Huang & Wyllie 1974). The diagrams show the calculated abundances of species with nonnegligible concentrations. The bulk solubility and the individual concentrations of total Si and Al increase with both pressure and temperature. In contrast, total K remains relatively constant with temperature but increases strongly with pressure. At all conditions portrayed, silica is the most abundant rock-forming oxide dissolved in H_2O, and both monomer and dimer species are important. Potassium is chiefly present as K^+ ions, with subordinate KOH ion pairs. Aluminum is predominantly $H_4AlO_4^-$, with subordinate neutral H_3AlO_3.

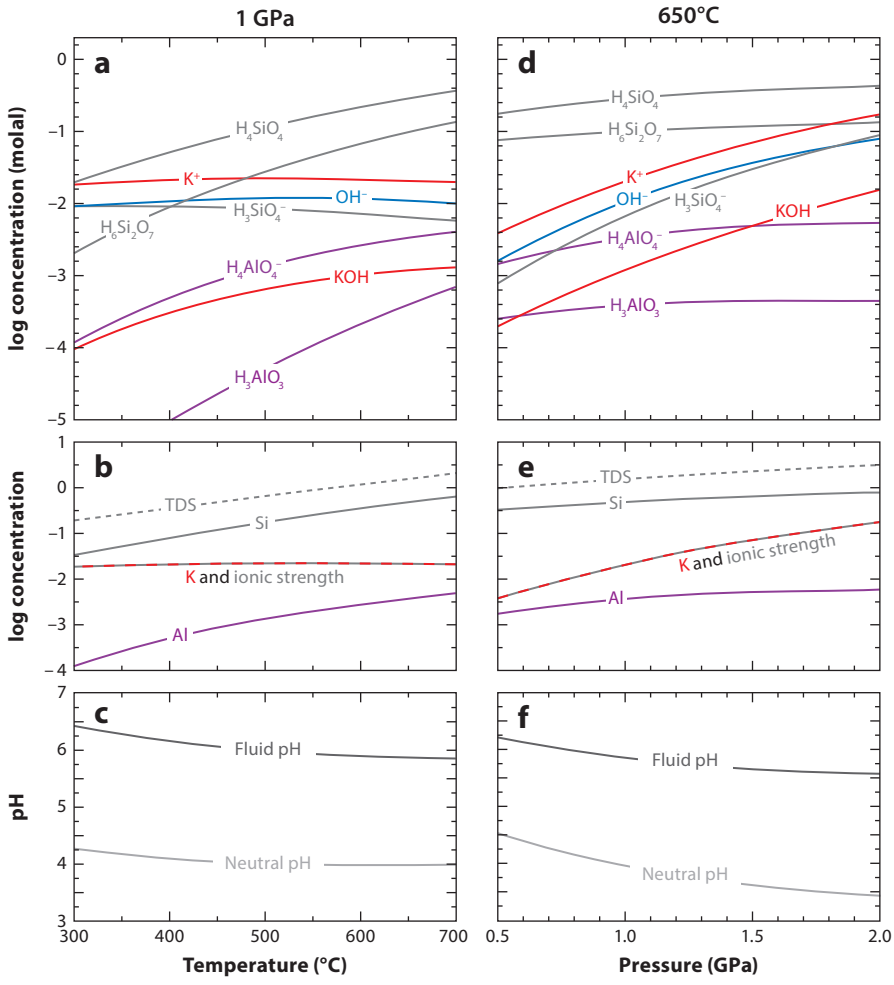

Figure 6

Model deep fluids resulting from equilibration of initially pure H_2O with muscovite + K feldspar + quartz (*a–c*) as a function of temperature at 1 GPa and (*d–f*) as a function of pressure at 650°C. Calculations are as in **Figure 4**, with thermodynamic data for minerals from Berman (1988). Panels *a* and *d* show species distributions (log molality): gray, Si species; red, K species; purple, Al species. In panels *b* and *e*, the *y* axes are log bulk concentrations [molality for elements and ionic strength; wt% oxides for total dissolved solids (TDS)]. Panels *c* and *f* show fluid pH and neutral pH.

As shown in **Figure 6*b,e***, the ionic strength of H_2O equilibrated with muscovite, K feldspar, and quartz is essentially equivalent to the K^+ concentration, because this ion is the most abundant in solution. The changes in ionic strength are consistent with variations in dielectric constant (**Figure 2*b***). Calculated total dissolved solids rise with both *T* and *P*. The pH (**Figure 6*c,f***) is everywhere significantly alkaline, which accounts for the abundance of Si and Al anions.

The system discussed above is highly simplified. Water equilibrated with natural rock compositions will contain element and species concentrations that vary with the assemblages and compositions of metamorphic minerals, which change with *P* and *T*. Galvez et al. (2015, 2016) computed the composition of H_2O equilibrated with pelite, basalt, and peridotite. Their results

are consonant with those reached above. Of particular note are the alkalis. In H_2O equilibrated with pelite and basalt there is a strong rise in Na^+ concentration with pressure, reaching a maximum at the albite = jadeite + quartz equilibrium and then declining at higher pressures. The concentrations of K^+ are more strongly dependent on changes in mineral assemblage.

In general, interaction between model rocks and H_2O free of Cl, C, or S produces mild to moderately alkaline pH; the large excursions from acid-base neutrality, as in ultramafic weathering, are not characteristic of deep-crustal fluid-rock interaction. Ionic strength of basalt- and ultramafic-equilibrated H_2O is lower than that for pelite. Total dissolved solids rise with *P* and *T*, are generally low, and are dominated by silica.

4. TOWARD MORE COMPLETE MODELS OF DEEP FLUIDS

The models above are useful for preliminary insights, but they yield poor approximations of actual deep-crustal fluids for several reasons. First, they are dilute, with low total dissolved solids, whereas all evidence from fluid inclusions and other sources points to deep-crustal fluids having much higher solute concentrations. Second, the activity of H_2O is near one. At many conditions in the deep crust, the presence of nearly pure H_2O will trigger melting. If fluids are present, the activity of H_2O must be less than one, typically significantly. Here I examine mechanisms by which solute load can be increased, and H_2O activity decreased, in the generation of more realistic deep-crustal fluids.

4.1. Carbon and Its Aqueous Species

Where the carbon content is set by interaction of H_2O with calcite at high fO_2, rising *P* and *T* yield strong increases in C concentration (Caciagli & Manning 2003, Kelemen & Manning 2015); the presence of alkali halides leads to even greater increases (Newton & Manning 2002a). In the presence of other silicate minerals, pH is set by calcite solubility through soluble Ca and C species, in many cases as ion pairs, such as $CaHCO_3^+$ (inferred by Sverjensky et al. 2014).

The solubility of calcite in H_2O is only ~3,000 ppm by weight at 700°C and 1 GPa (Caciagli & Manning 2003). Fluids with tens of mole percent CO_2 must derive their carbon by other means (see the sidebar titled Sources of Fluid Components). At these higher concentrations of CO_2, silicate

SOURCES OF FLUID COMPONENTS

A key problem for lower-crustal fluids remains the sources of chloride and gases such as CO_2. Fluid-rock reactions during carbonate metamorphism can produce CO_2-rich fluid; however, carbonates are not typically present in sufficient quantities to have more than a local effect. Commonly cited sources of chloride in deep-crustal fluids are dissolution of chloride-bearing minerals and preferential partitioning of H_2O relative to halide during hydration reactions (Manning & Aranovich 2014, Yardley & Graham 2002). But Cl-bearing minerals are not especially common, and the latter process requires very large extents of reaction to be effective; one possibility may be fluids with very long travel paths, as may be indicated by the G anomaly. Two additional mechanisms are likely more important than has previously been understood. First, there is growing appreciation of the importance of magmatic inputs into the lower crust; stalled magmas become fluid saturated in the lower crust, and the fluid produced is rich in low-solubility components CO_2 and Cl. In addition, immiscibility in the H_2O-CO_2-salt system (**Figure 1**) means that, upon unmixing of a single fluid, the separate fluid phases become relatively enriched in salt and CO_2 components.

mineral solubility drops strongly due to the reduction in H_2O activity and dielectric constant. CO_2 acts as an inert diluent, causing quartz solubility to decline with H_2O activity (Newton & Manning 2000, 2009; Shmulovich et al. 2006). This is because dissolved silica is a hydroxide species. In the absence of any SiO_2-CO_2 interaction, reduction in H_2O activity shifts Equation 6 to the left, decreasing quartz solubility and yielding a fluid that is comparatively low in dissolved solutes. Similar results are seen for other silicate minerals (Shmulovich et al. 2001). In general, CO_2-rich fluids are poor solvents and contribute little to conductivity or metasomatic mass transfer of major elements.

4.2. Chloride and Other Anions

As shown in **Figure 1**, chloride concentrations range from dilute to strongly concentrated brines. Chloride has a profound effect on chemistry and properties of aqueous solutions (Eugster 1981, Eugster & Baumgartner 1987, Eugster & Gunter 1981, Helgeson 1969, Yardley & Bodnar 2014). **Figure 7** shows the role of modest chlorinity on H_2O-rock interaction, for the assemblage muscovite + K feldspar + quartz. At the lowest Cl concentrations, absolute and relative species concentrations are similar to those in pure H_2O (cf. **Figure 6**). However, this changes when Cl concentration becomes subequal to K concentration. Because potassium is predominantly K^+ and chlorine is predominantly Cl^-, addition of Cl^- in excess of the K^+ generated by mineral dissolution requires additional K from the mineral assemblage to balance the negative charge. Hence, above about 0.01 molal Cl_{total}, the solution is dominated by K^+ and KCl, and other anions decrease in concentration. The trends in total dissolved solids and pH are similar to those determined experimentally at low *P* (Hauzenberger et al. 2001); however, solute concentrations are much greater at high *P*. Mineral assemblage plays a role in pH control. For example, the presence of kyanite instead of K feldspar decreases pH by ~0.3–0.5 units (**Figure 7*c***).

Sulfide minerals are common in metamorphic rocks and provide a source for dissolved sulfur species. Adding magnetite + pyrrhotite + pyrite to muscovite + K feldspar + quartz yields total dissolved sulfur of 2.0 molal in chloride-free fluids at 700°C and 1 GPa. H_2S and HSO_4^- are the dominant dissolved species, though the model does not account for S_3^-, which may be abundant (Pokrovski & Dubrovinsky 2011). The pH is 5.3—less alkaline than in the sulfur-free system, illustrating how the presence of additional anions pulls the pH toward neutrality. Increasing total chloride does not change predominant species, but total S declines in response to the decreasing pH.

Higher concentrations of alkali halides strongly affect mineral solubility in deep-crustal fluids (Manning & Aranovich 2014). The electrolyte activity coefficient model employed in these calculations is valid only to ~3 molal. At higher salinity, experimental studies provide important insights and show that mineral solubility in brines depends on mineral composition and structure. At fixed lower-crustal *P* and *T*, alkali halide salts are mostly dissociated (Aranovich & Newton 1996, 1997). Quartz solubility generally decreases with rising salt concentration (Newton & Manning 2000); however, the decline is less pronounced than for CO_2 (Newton & Manning 2009), and solubility may actually increase slightly at the lowest concentrations of some salts (Shmulovich et al. 2006). This could be due to changes in solvent properties (Shmulovich et al. 2001, 2006; Xie & Walther 1993) or complexing of salt components with silica (Evans 2007, Newton & Manning 2016). In any case, the general decrease in quartz solubility for a given reduction in a_{H_2O} by salt addition is much less than that for CO_2 (Newton & Manning 2000, 2009, 2010). Thus, low-a_{H_2O} brines are better solvents for silica than low-a_{H_2O} fluids containing only CO_2. Of coexisting fluids in the H_2O-CO_2-salt system (**Figure 1**), the brine phase should therefore be expected to contain more SiO_2 than the CO_2-rich phase.

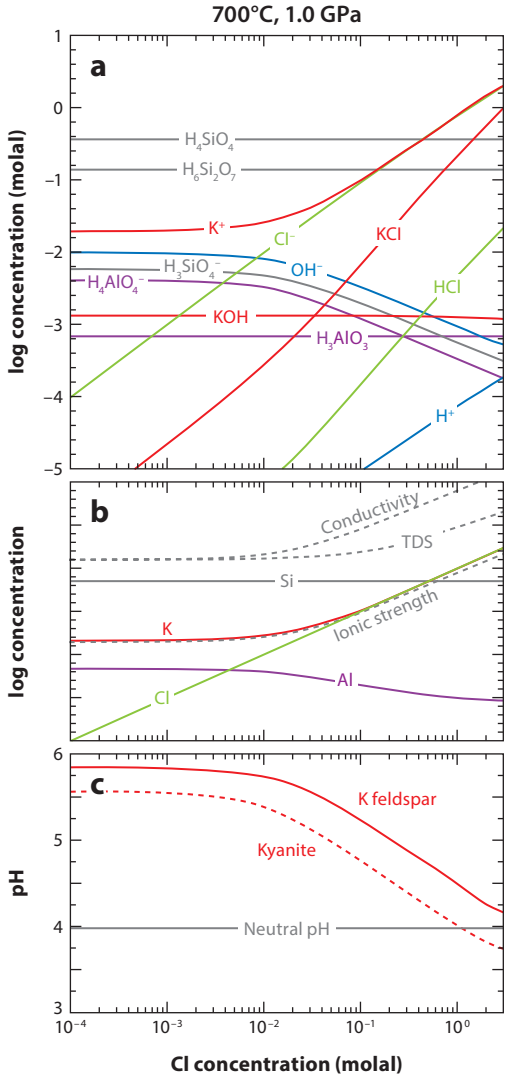

Figure 7

Model deep fluids resulting from equilibration of H_2O with muscovite + K feldspar + quartz at 700°C and 1.0 GPa as a function of Cl concentration. Calculations are as in **Figure 4**. (*a*) Species distributions (log molality), with colors as in **Figure 6** except for green, which represents Cl species; (*b*) log bulk concentrations and log conductivity [molality for elements and ionic strength; wt% oxides for total dissolved solids (TDS); S/m for conductivity (σ_f, using the model of Foustoukos 2016)]; (*c*) fluid pH and neutral pH. Also shown in panel *c* is the pH variation if kyanite is substituted for K feldspar in the assemblage (*red dashed line*). The equation of Foustoukos (2016) for fluid conductivity is strictly applicable to salt $m_{NaCl} > 0.6$; it is used here to facilitate comparison with changing salinity. Other simple methods yield lower values of σ_f at low salinity.

Shimojuku et al. (2012, 2014) determined electrical conductivity of H_2O-NaCl solutions in quartzite at an effective porosity of ~0.2–0.3. Their measured conductivities are lower than expected from Sakuma & Ichiki's (2016b) and Sinmyo & Keppler's (2017) models, once porosity is taken into account. Lower conductivity could arise from the SiO_2-NaCl complexing proposed by Newton & Manning (2016).

Makhluf et al. (2016) showed that the solubility of albite in H_2O-NaCl also declines with rising salt concentration. However, in contrast to those of quartz and albite, the solubilities of other oxide minerals in H_2O-NaCl (e.g., corundum or wollastonite) at a given high *P* and *T* initially increase with salt concentration to modest mole fractions, reach a maximum, and then decline (Newton & Manning 2006, 2008a). Garnet is common in the lower crust. Newton & Manning (2007) showed that the solubility of grossular ($Ca_3Al_2Si_3O_{12}$) in NaCl at 800°C and 10 kbar is higher than in pure H_2O at all NaCl mole fractions, and that it dissolves congruently to produce a salt-rich solution with molar Ca/Al = 3/2. Evidently the Al concentration of lower-crustal brines can be quite high. Solubility patterns imply that the solute species are complex mixtures of metal-chloride ions (e.g., $CaCl^+$) and sodium aluminosilicate species (Newton & Manning 2010).

Minerals with more strongly ionic character have higher solubility than oxide minerals. For example, at fixed *P* and *T*, the solubilities of calcite ($CaCO_3$), anhydrite ($CaSO_4$), fluorite (CaF_2), and apatite [$Ca_5(PO_4)_3$] increase exponentially with increasing NaCl to a maximum at halite saturation (Manning & Aranovich 2014, Newton & Manning 2010). Inferred solutes are Ca chlorides and Na-anion pairs.

In general, saline fluids in the deep crust produce lower quartz solubility than pure H_2O, though it is elevated relative to H_2O-CO_2. Other oxides exhibit surprising increases in solubility with salt concentration, and the solubilities of carbonates, sulfates, and phosphates are high to extreme. Thus, at all deep-crustal conditions, highly saline solutions contain substantially more solutes derived from their host rocks (**Figure 1**); that is, they are more effective agents of metasomatic mass transfer.

4.3. Aluminosilicate Polymerization

The tendency of solute silica to polymerize has important implications for other cations, especially aluminum. Aluminum readily substitutes for Si in the rock-forming silicate minerals and combines with silica to form polymerized networks in silicate melts. It has a similar role in deep-crustal aqueous solutes in that it displays a strong capacity to combine with silica to generate a range of oligomeric structures. As with Si, highly polymerized Al is known at ambient conditions at extremes in pH where Al concentration may be high. At high *P* and *T*, Al concentration in corundum-saturated H_2O is modest (Tropper & Manning 2007), and alumina does not detectibly polymerize with itself (Mookherjee et al. 2014). However, Al interactions with silica are extensive at deep-crustal conditions and lead to dramatically higher aqueous Al concentrations (Manning 2007).

The effects of this polymerization are profound but poorly quantified. The key to understanding their importance for deep-crustal fluids is to compare predicted solubilities, as in the examples above, to those observed experimentally. In the absence of aluminosilicate polymerization, as in near-neutral shallow-crustal fluids, Al solubility in H_2O is generally quite low. At saturation with aluminous minerals such as corundum (Al_2O_3) and and/or sillimanite (Al_2SiO_5), increasing aqueous Si concentration yields no change or a decrease in Al concentration. However, in experiments at 1 GPa and 700°C, Manning (2007) found that Al concentrations in H_2O equilibrated with kyanite + corundum were greater than predicted assuming no Si-Al interaction. The excess Al solubility (by a factor of about five) is a consequence of aluminosilicate polymerization. In general, Al-Si interaction via polymerization leads to an increase in Al solubility with Si concentration, such that it reaches a maximum at quartz saturation. This helps explain common observations of Al-rich minerals in deep-crustal veins and leads to the surprising conclusion that, unlike in shallow systems, Al may be one of the most abundant solutes in deep fluids.

Further evidence comes from the results of Manning et al. (2010), who determined the solubility of albite + paragonite + quartz at 350–620°C and 10 kbar (**Figure 8**). Measured solubilities

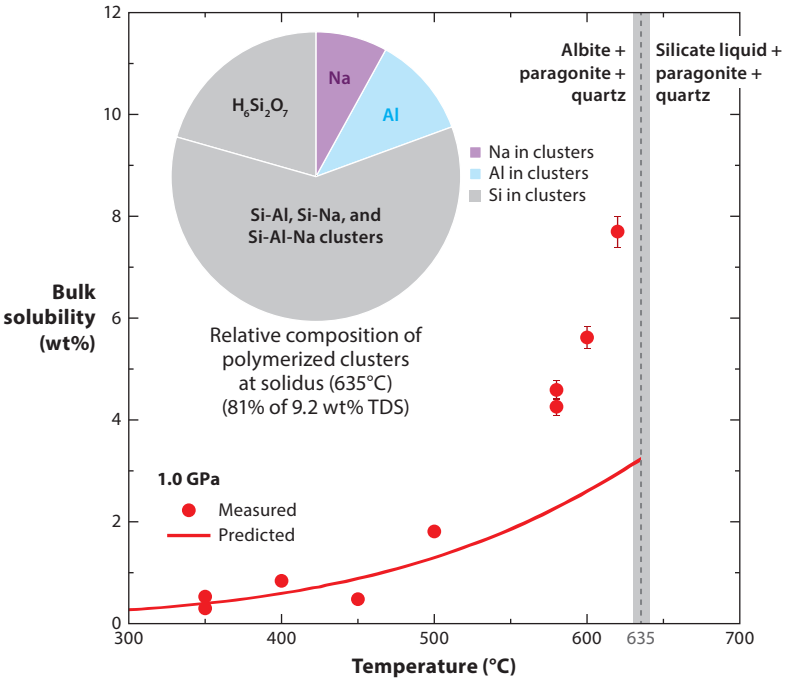

Figure 8

Comparison of predicted and experimentally determined solubilities of albite + paragonite + quartz at 1.0 GPa. Panel modified from Manning et al. (2010). Red circles show experimental measurements; the red line indicates solubility predicted considering only ionic solutes, neutral monomers and ion pairs, and the silica dimer. Divergence of measured bulk solubility from calculated values signals the presence of polymerized Al-Si species not taken into account in the model. The data show that the abundance of polymerized species grows with rising temperature until the solidus is reached at 635°C (*gray dashed line*; uncertainty indicated by *gray band*), above which a hydrous silicate liquid is stable. The predicted composition of polymerized species (clusters) at the solidus (635°C) is shown in the inset. Polymerized clusters constitute 81% (7.5 wt%) of total dissolved solids (TDS).

agree with those predicted at 350°C to ~500°C, confirming that simple ions, monomers, and ion pairs of species accurately reproduce observations. However, from 500°C to 620°C, observed solubilities are greater than those derived from models using unpolymerized solutes (**Figure 8**). The discrepancy grows with T to the melting point. The divergence between predicted and observed composition is due to a growing concentration of Al-Si polymeric clusters excluded from the calculations because of the absence of thermodynamic data. In fact, these species are the most abundant solutes at these conditions. For example, at the wet solidus, the concentration of polymerized clusters is 7.5 wt%, or 81% of the total solute load of 9.2 wt%. Most such species must be Si-Al, Si-Na, and Si-Al-Na oxide clusters. Preliminary indications based on electrical conductivity measurements suggest that the polymerized species are mostly neutral complexes (Guo et al. 2015). Aluminum and sodium have subequal concentrations on a molar basis.

The concentrations of polymerized solutes in H_2O becomes so high at elevated P and T that complete miscibility between silicate melts and H_2O may be attained (Manning 2004, 2017). The supercritical fluids thus produced tend to be stable at the higher pressures of the upper mantle; however, key chemical systems in which complete miscibility may be accessible at lower-crustal

conditions include quartz-H_2O and albite-H_2O (Hayden & Manning 2011, Kennedy et al. 1962, Makhluf et al. 2016, Shen & Keppler 1997). In each case, addition of CO_2 and/or salt destabilizes the supercritical fluid and causes phase separation (Cruz & Manning 2015, Makhluf et al. 2016).

5. DEEP FLUIDS AND CRUSTAL MELTING

Both CO_2 and salts suppress lower-crustal melting by virtue of the reduction in H_2O activity; however, for the same molar concentration, salts do so to a greater degree than CO_2. This arises from the different activity-concentration relations along the two binary joins (Manning & Aranovich 2014, Newton et al. 1998). At 1.0 GPa, H_2O-saturated melting of simple granite occurs at ~640°C. Addition of 50 mol% CO_2 raises melting T to 710°C, whereas the same concentration of NaCl + KCl yields melting at 845°C (Aranovich et al. 2013). Thus, in the presence of salt-rich solutions, melting by the common mechanism of biotite dehydration is suppressed below 800°C at lower-crustal pressures (Aranovich & Newton 1998, Newton et al. 2014).

Emerging models of magmatic systems in tectonically active crust highlight the importance of magmas stalling at different crustal levels, where they may degas, and assimilate or melt surrounding crust (e.g., Annen et al. 2006, Cashman et al. 2017). The contributions of degassed components to crustal metamorphic fluids, and the complex mixing/unmixing they could induce, have received insufficient attention. They may be critical to evaluating the deep-crustal fluid-rock interaction in many settings.

6. RECONCILING MODELS AND OBSERVATIONS

Vein assemblages in metamorphic rocks exhumed from the lower crust have long posed a dilemma. The components forming the vein minerals must be soluble in the fracture-filling fluid to explain the requisite material transport. Veins filled solely by quartz are easily explained by high Si solubility. However, refractory Al-rich silicates like kyanite, staurolite, and garnet are common accessories (e.g., Ague 1995). It is difficult to explain with current thermodynamic models the precipitation of such Al-rich minerals because Al solubility in pure H_2O and chloride solutions, as in the examples discussed above, is low at the conditions explored. However, incorporation of Al via aluminosilicate polymers readily explains aluminous vein minerals. Generally, Al is more soluble than many monovalent and divalent cations, at least in low-Cl solutions, and aluminosilicate vein minerals should in fact be expected in metamorphic rocks exhumed from >0.5 GPa.

Whereas the veins in metamorphic rocks provide insight into fluid-rock interaction in the geologic past, resistivity surveys give information on zones of currently active lower-crustal metamorphism. Anomalies commonly interpreted to indicate the presence of a fluid phase may reach bulk conductivities of 0.05 to 1 S/m. Can such conductivity anomalies be reconciled with theoretical and experimental fluid compositions discussed above?

Figure 9 shows conductivity at lower-crustal depths, highlighting the range of high observed bulk conductivity found in many studies, including the G anomaly (Worzewski et al. 2011). The bulk conductivity of a model crustal rock composed of muscovite + K feldspar + quartz can be calculated from the ionic strength predicted by the DEW model and Equation 5. The calculation employed a 15°C/km linear geotherm, rock density of 2,800 kg/m^3, and the cube model for bulk conductivity (Waff 1974). Calculation of bulk conductivity requires as input the porosity of lower-crustal rocks during metamorphism, which is neither constant nor known with certainty. Previous analyses of bulk conductivity commonly used porosity as the main independent variable, but the values considered vary by orders of magnitude and in many cases are assumed to be at least 0.01.

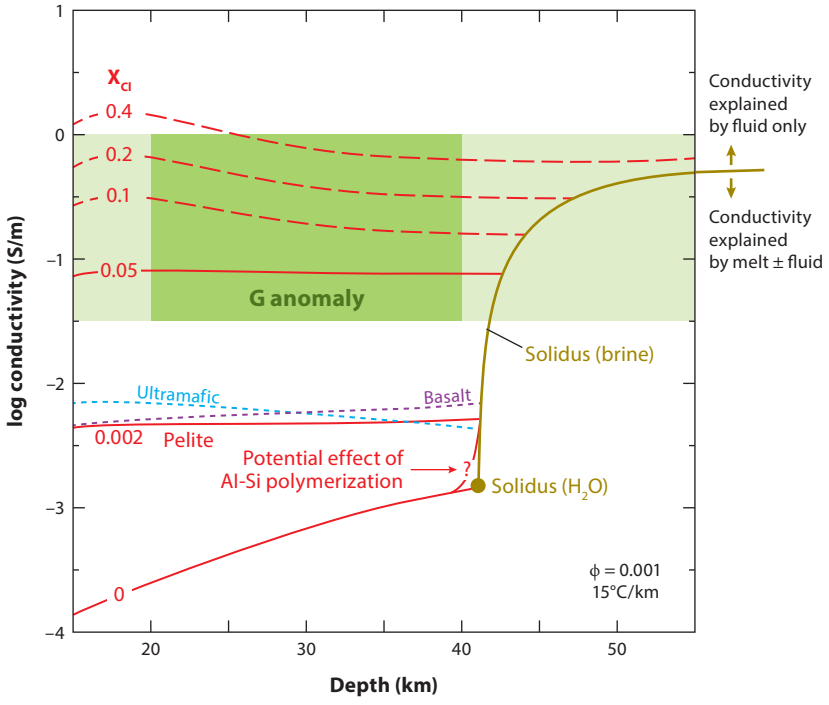

Figure 9

Conductivity-depth relations for model deep-crustal fluids. The light green field shows the range of bulk conductivity associated with lower-crustal anomalies in a range of settings. The depth-conductivity range of the G anomaly (e.g., Worzewski et al. 2011) is shown in dark green. Lines show bulk conductivity (σ_B) along a 15°C/km geothermal gradient (density = 2,800 kg/m^3), as derived from calculated ionic strength I (Equation 5) based on equilibration of H_2O with the model mineral assemblage, as in **Figure 6**, and converting fluid to bulk conductivity using the cube model for rock porosity (ϕ) of 0.001. Solid red lines denote fluids with 0, 0.1, and 3.0 molal total Cl (X_{Cl} = 0, 0.002, 0.05, respectively, neglecting other solutes) equilibrated with model pelite comprising muscovite + K feldspar + quartz. Short-dashed lines correspond to σ_B at 0.1 molal total Cl total fluid in model basalt (diopside + albite + clinozoisite + quartz; *purple*) and ultramafic (talc + forsterite; *light blue*) assemblages. Long-dashed red lines were derived by considering only H_2O-NaCl solutions; at these high salinities, contributions from other dissolved solutes are negligible. The dark yellow line shows the melting curve of a model simple granite, which increases in temperature with rising salt content (Aranovich et al. 2013); conductivity isopleths are terminated at the solidus for clarity, illustrating the boundary between crust in which bulk conductivity can be explained by the presence of saline fluid alone and that in which melt and saline fluid may both contribute. The queried red line at X_{Cl} = 0 shows the possible effect of charged polymerized solutes on bulk conductivity assuming 50% of species are monovalent.

Such high porosities are more likely associated with dynamic expulsion of metamorphic fluid (e.g., Connolly 1997, 2010; Thompson & Connolly 1990). Lower porosity values should be used where fluids are present but not being actively expelled, the likely scenario for conductivity surveys. Estimates of porosity in this case are 10^{-3} or less (e.g., Ague 2014, Connolly 2010, Skelton et al. 2000). The upper value is used here for illustration.

The conductivity of a Cl-free fluid rises with depth (and T) but remains well below the values indicated by conductivity anomalies over the depth interval of interest (**Figure 9**). Of the many models relating ionic strength to conductivity, the recent one of Foustoukos (2016) is used here.

Though strictly applicable to chloride solutions, it is employed even for Cl-free solutions for three reasons: (*a*) for consistency with calculations in chloride solutions below; (*b*) because it returns higher (and in the present context more conservative) conductivity than other simple models; and (*c*) because errors should be small at the scale of conductivity portrayed. In the presence of Cl-free H_2O, this bulk composition will melt at 41 km depth along the modeled geotherm (Huang & Wyllie 1974). It is likely that the solubility of aluminosilicate complexes will increase dramatically within 50°C (~3 km) of the solidus. If the increase is similar to the albite-paragonite-quartz system (Manning et al. 2010), then ~7 wt% excess total dissolved solids can be expected as polymerized aluminosilicate species not accounted for in the DEW model. Some of this solute must be ionized. However, even if half of all excess alkalis and Al are present in monovalent species, the resulting conductivity would rise only to 0.007 S/m (**Figure 9**).

Adding Cl so that $Cl_{total} = 0.1$ molal (equivalent to KCl mole fraction of 0.002) yields elevated solubility and raises conductivity to an approximately depth-independent value of ~0.005 S/m. Most of the ionic strength is due to K^+ and Cl^-, but other ions contribute to a subordinate degree. This can be seen by comparing the conductivities of model pelite with model basalt and ultramafic at the same bulk Cl_{total} (**Figure 9**). The slightly different bulk conductivities and trends with depth arise from the differing concentrations of cations in the chloride solution. Yet, regardless of rock composition or crustal level, the bulk conductivity remains <0.01 S/m at this porosity.

Figure 9 shows that increasing Cl_{total} above ~1 molal yields bulk conductivity within the range of anomalies observed in tectonically active lower crust. At these salinities, there is effectively no dependence on depth or temperature, and additional solutes other than K^+ and Cl^- contribute <1% to the conductivity (**Figure 7**). Thus, only bulk salt content is relevant. Conductivities for more concentrated solutions at the same porosity are also shown. If CO_2 is present, it will decrease conductivity, but compositions along the brine limb of the solvus possess CO_2 concentrations that are insufficient to change the conclusions. Although the focus in this is example is the G anomaly, it is important to note that the effect of high salinity at higher temperature is to suppress melting (Aranovich et al. 2013). **Figure 9** illustrates the change in solidus temperature that attends increasing salinity in the coexisting fluid. High conductivity in deep environments in which temperature is greater than that of H_2O-saturated melting (e.g., some portions of the Tibetan crust) is often attributed to the presence of a silicate melt. However, this observation could also be explained by the presence of an alkali-chloride solution, which reduces H_2O activity sufficiently to keep the rocks from melting (**Figure 9**).

A requirement of bulk conductivity models is that the conductive phase is interconnected, which in the case of lower-crustal fluids necessitates grain-boundary or edge wetting (e.g., Waff 1974). This is readily achieved for saline fluids, but not for CO_2-rich fluids (e.g., Gibert et al. 1998). Results of resistivity surveys also imply that lower-crustal fluids are present for extended times. While individual outcrops may suggest very short durations of fluid flow, when averaged over the scale of resolution of magnetotelluric data, it is plausible that fluids are continuously present in such volumes on timescales of 10^6 years or more (Ague 2014). Thus, the results summarized in **Figure 9** offer compelling evidence that geophysical and geochemical data are converging to reveal the presence and composition of fluids in areas of active lower-crustal metamorphism.

SUMMARY POINTS

1. Deep fluids are distinct from their shallow counterparts in that they are composed of less H_2O and more salts, gases, and rock solutes; consequently, the activity of H_2O in the fluid phase is never one, and in many cases may be substantially lower than one.

2. A miscibility gap in the H_2O-salt-gas ternary system can cause separation into two fluid phases with different chemical and physical properties. Differences in wetting properties cause CO_2-rich fluids to be overrepresented in fluid inclusions, while salt-rich fluid inclusions are rare. Yet salt-rich fluids control the chemistry of fluid-rock interaction.
3. Deep fluids are relatively incompressible, and their dielectric constant is reduced by addition of CO_2 and salt. Neutral pH is typically <4.5, with a maximum increase of ~0.5 in CO_2- or salt-rich solutions. Conductivity variations are controlled primarily by salt concentration; there is little change with P and T for a given salinity.
4. Rising P and T increase the bulk solubility of typical crustal rocks in H_2O. Chloride further enhances solubility, but CO_2 has the opposite effect. H_2O-salt fluids alone have slightly alkaline pH at high P and T, as does H_2O equilibrated with rock-forming minerals. However, progressive increase in salinity in the presence of minerals yields decreasing pH; deep saline fluids can be neutral to mildly acidic depending on the composition of their host.
5. Silica is the most abundant solute in H_2O-rich fluids, due in part to its ability to polymerize. Al-Si interactions raise Al solubility significantly. Current thermodynamic data are insufficient to capture many of these effects, leading models to underpredict total dissolved aluminosilicate—by up to 80% by weight—in the deep crust, especially near fluid-saturated melting conditions. Extensive polymerization promotes critical mixing of H_2O-silicate systems.
6. Deep fluid conductivity is low in H_2O- or CO_2-rich fluids; however, the bulk conductivities associated with deep-crustal resistivity anomalies are readily produced by salty solutions of even modest salinity and reasonable porosities.

FUTURE ISSUES

1. New quantitative thermodynamic models and data on more complex, polymerized solutes hold the key for improving our understanding of the chemistry of deep-crustal fluids.
2. It is critical to exploit or develop geochemical tools for investigating the nature of the liberation of magmatic fluids and their interaction with metamorphic fluids and rocks in the deep crust.
3. The conceptual models of crustal fluids currently deployed by petrologists and geophysicists are in conflict. The former typically envision dynamic, rapid expulsion from an otherwise largely dry crust, whereas the latter provide data that seem to imply the steady-state presence of fluid in important metamorphic settings. Lowering time- and volume-averaged porosity can reduce the disparity. Thus, at a minimum, better understanding of hydrologic parameters and their dynamics, especially porosity and permeability, are central to making progress on this problem.
4. While it is now clear that fluids of moderate salinity can explain some conductivity anomalies, the sources of salinity (and other constituents such as CO_2) remain largely unknown.

DISCLOSURE STATEMENT

The author is not aware of any affiliations, memberships, funding, or financial holdings that might be perceived as affecting the objectivity of this review.

ACKNOWLEDGMENTS

This review has benefited from discussions and collaborations with numerous colleagues, but R.C. Newton deserves special mention. It has been a privilege to collaborate and share our enthusiasm for all aspects of deep fluids. The manuscript was prepared while I benefited from the generous support of the Institut de Physique du Globe de Paris. The work was supported by the Deep Carbon Observatory and National Science Foundation grants EAR-1347987 and EAR-1732256.

LITERATURE CITED

Abramson EH, Brown JM. 2004. Equation of state of water based on speeds of sound measured in the diamond-anvil cell. *Geochim. Cosmochim. Acta* 68:1827–35

Ague JJ. 1991. Evidence for major mass transfer and volume strain during regional metamorphism of pelites. *Geology* 19:855–58

Ague JJ. 1994a. Mass transfer during Barrovian regional metamorphism of pelites, south-central Connecticut: I. Evidence for changes in composition and volume. *Am. J. Sci.* 294:989–1057

Ague JJ. 1994b. Mass transfer during Barrovian regional metamorphism of pelites, south-central Connecticut: II. Channelized fluid flow and the growth of staurolite and kyanite. *Am. J. Sci.* 294:1061–134

Ague JJ. 1995. Deep crustal growth of quartz, kyanite and garnet into large-aperture, fluid-filled fractures, north-eastern Connecticut, USA. *J. Metamorph. Geol.* 13:299–314

Ague JJ. 2014. Fluid flow in the deep crust. In *Treatise on Geochemistry*, Vol. 4: *The Crust*, ed. HD Holland, KK Turekian, pp. 203–47. Oxford, UK: Elsevier. 2nd ed.

Anderson GM, Burnham CW. 1965. The solubility of quartz in supercritical water. *Am. J. Sci.* 263:494–511

Anderson GM, Castet S, Schott J, Mesmer RE. 1991. The density model for estimation of thermodynamic parameters of reactions at high temperatures and pressures. *Geochim. Cosmochim. Acta* 55:1769–79

Annen C, Blundy J, Sparks R. 2006. The genesis of intermediate and silicic magmas in deep crustal hot zones. *J. Petrol.* 47:505–39

Aranovich LY, Newton RC. 1996. H_2O activity in concentrated NaCl solutions at high pressures and temperatures measured by the brucite-periclase equilibrium. *Contrib. Mineral. Petrol.* 125:200–12

Aranovich LY, Newton RC. 1997. H_2O activity in concentrated KCl and KCl-NaCl solutions at high temperatures and pressures measured by the brucite-periclase equilibrium. *Contrib. Mineral. Petrol.* 127:261–71

Aranovich LY, Newton RC. 1998. Reversed determination of the reaction: phlogopite + quartz = enstatite + potassium feldspar + H_2O in the ranges 750–875°C and 2–12 kbar at low H_2O activity with concentrated KCl solutions. *Am. Mineral.* 83:193–204

Aranovich LY, Newton RC, Manning CE. 2013. Brine-assisted anatexis: experimental melting in the system haplogranite-H_2O-NaCl-KCl at deep-crustal conditions. *Earth Planet. Sci. Lett.* 374:111–20

Aranovich LY, Zakirov IV, Sretenskaya NG, Gerya TV. 2010. Ternary system H_2O-CO_2-NaCl at high *T-P* parameters: an empirical mixing model. *Geochem. Int.* 48:446–55

Artemieva IM, Mooney WD. 2001. Thermal thickness and evolution of Precambrian lithosphere: a global study. *J. Geophys. Res.* 106:16387–414

Aso N, Ohta K, Ide S. 2013. Tectonic, volcanic, and semi-volcanic deep low-frequency earthquakes in western Japan. *Tectonophysics* 600:27–40

Audétat A, Keppler H. 2005. Solubility of rutile in subduction zone fluids, as determined by experiments in the hydrothermal diamond anvil cell. *Earth Planet. Sci. Lett.* 232:393–402

Bai D, Unsworth MJ, Meju MA, Ma X, Teng J, et al. 2010. Crustal deformation of the eastern Tibetan plateau revealed by magnetotelluric imaging. *Nat. Geosci.* 3:358–62

Bali E, Audétat A, Keppler H. 2013. Water and hydrogen are immiscible in Earth's mantle. *Nature* 495:220–22

Bassett WA, Shen A, Bucknum M, Chou IM. 1993. A new diamond anvil cell for hydrothermal studies to 2.5 GPa and from −190 to 1200°C. *Rev. Sci. Instrum.* 64:2340–45

Becken M, Ritter O. 2012. Magnetotelluric studies at the San Andreas Fault Zone: implications for the role of fluids. *Surv. Geophys.* 33:65–105

Becker KH, Cemic L, Langer KEOE. 1983. Solubility of corundum in supercritical water. *Geochim. Cosmochim. Acta* 47:1573–78

Berman RG. 1988. Internally-consistent thermodynamic data for minerals in the system Na_2O-K_2O-CaO-MgO-FeO-Fe_2O_3-Al_2O_3-SiO_2-TiO_2-H_2O-CO_2. *J. Petrol.* 29:445–522

Beroza GC, Ide S. 2011. Slow earthquakes and nonvolcanic tremor. *Annu. Rev. Earth Planet. Sci.* 39:271–96

Caciagli NC, Manning CE. 2003. The solubility of calcite in water at 6–16 kbar and 500–800°C. *Contrib. Mineral. Petrol.* 146:275–85

Cashman KV, Sparks RSJ, Blundy JD. 2017. Vertically extensive and unstable magmatic systems: a unified view of igneous processes. *Science* 355:eaag3055

Chen L, Booker JR, Jones AG, Wu N, Unsworth MJ, et al. 1996. Electrically conductive crust in southern Tibet from INDEPTH magnetotelluric surveying. *Science*: 274:1694–96

Chervin J, Canny B, Besson J, Pruzan P. 1995. A diamond anvil cell for IR microspectroscopy. *Rev. Sci. Instrum.* 66:2595–98

Connolly JAD. 1997. Devolatilization-generated fluid pressure and deformation-propagated fluid flow during prograde regional metamorphism. *J. Geophys. Res.* 102:18149–73

Connolly JAD. 2010. The mechanics of metamorphic fluid expulsion. *Elements* 6:165–72

Crawford ML, Hollister LS. 1986. Metamorphic fluids: the evidence from fluid inclusions. In *Fluid-Rock Interactions During Metamorphism*, ed. JV Walther, BJ Wood, pp. 1–35. New York: Springer-Verlag

Cruz MF, Manning CE. 2015. Experimental determination of quartz solubility and melting in the system SiO_2-H_2O-NaCl at 15–20 kbar and 900–1100°C: implications for silica polymerization and formation of supercritical fluids. *Contrib. Mineral. Petrol.* 170:35

Dipple GM, Ferry JM. 1992. Metasomatism and fluid flow in ductile fault zones. *Contrib. Mineral. Petrol.* 112:149–64

Dolejš D. 2013. Thermodynamics of aqueous species at high temperatures and pressures: equations of state and transport theory. *Rev. Mineral. Geochem.* 76:35–79

Dolejš D, Manning CE. 2010. Thermodynamic model for mineral solubility in aqueous fluids: theory, calibration and application to model fluid-flow systems. *Geofluids* 10:20–40

Duan ZH, Zhang ZG. 2006. Equation of state of the H_2O, CO_2, and H_2O-CO_2 systems up to 10 GPa and 2573.15 K: molecular dynamics simulations with ab initio potential surface. *Geochim. Cosmochim. Acta* 70:2311–24

Etheridge MA, Wall VJ, Vernon RH. 1983. The role of the fluid phase during regional metamorphism and deformation. *J. Metamorph. Geol.* 1:205–26

Eugster HP. 1981. Metamorphic solutions and reactions. *Phys. Chem. Earth* 13:461–507

Eugster HP, Baumgartner L. 1987. Mineral solubilities and speciation in supercritical metamorphic fluids. *Rev. Mineral.* 17:367–403

Eugster HP, Gunter WD. 1981. The compositions of supercritical metamorphic solutions. *Bull. Mineral.* 104:817–26

Evans K. 2007. Quartz solubility in salt-bearing solutions at pressures to 1 GPa and temperatures to 900°C. *Geofluids* 7:451–67

Evans RL, Wannamaker PE, McGary RS, Elsenbeck J. 2014. Electrical structure of the central Cascadia subduction zone: the EMSLAB Lincoln Line revisited. *Earth Planet. Sci. Lett.* 402:265–74

Ferry JM. 1994. A historical review of metamorphic fluid flow. *J. Geophys. Res.* 99:15487–98

Ferry JM, Baumgartner L. 1987. Thermodynamic models of molecular fluids at the elevated pressures and temperatures of crustal metamorphism. *Rev. Mineral.* 17:323–65

Foustoukos DI. 2016. On the ionic strength and electrical conductivity of crustal brines. *Chem. Geol.* 447:183–90

Foustoukos DI, Mysen BO. 2012. D/H fractionation in the H_2-H_2O system at supercritical water conditions: compositional and hydrogen bonding effects. *Geochim. Cosmochim. Acta* 86:88–102

Frantz JD. 1998. Raman spectra of potassium carbonate and bicarbonate aqueous fluids at elevated temperatures and pressures: comparison with theoretical simulations. *Chem. Geol.* 152:211–25

Frantz JD, Dubessy J, Mysen B. 1993. An optical cell for Raman spectroscopic studies of supercritical fluids and its application to the study of water to 500°C and 2000 bar. *Chem. Geol.* 106:9–26

Frantz JD, Dubessy J, Mysen BO. 1994. Ion-pairing in aqueous $MgSO_4$ solutions along an isochore to 500°C and 11 kbar using Raman spectroscopy in conjunction with the diamond-anvil cell. *Chem. Geol.* 116:181–88

Frost BR, Bucher K. 1994. Is water responsible for geophysical anomalies in the deep continental crust? *Tectonophysics* 231:293–309

Fyfe WS, Price NJ, Thompson AB. 1978. *Fluids in the Earth's Crust*. Amsterdam: Elsevier

Galvez ME, Connolly JAD, Manning CE. 2016. Implications for metal and volatile cycles from the pH of subduction zone fluids. *Nature* 539:420–24

Galvez ME, Manning CE, Connolly JAD, Rumble D. 2015. The solubility of rocks in metamorphic fluids: a model for rock-dominated conditions to upper mantle pressure and temperature. *Earth Planet. Sci. Lett.* 430:486–98

Gerya TV, Maresch WV, Burchard M, Zakhartchouk V, Doltsinis NL, Fockenberg T. 2005. Thermodynamic modeling of solubility and speciation of silica in H_2O-SiO_2 fluid up to 1300°C and 20 kbar based on the chain reaction formalism. *Eur. J. Mineral.* 17:269–83

Gibert F, Guillaume D, Laporte D. 1998. Importance of fluid immiscibility in the H_2O-NaCl-CO_2 system and selective CO_2 entrapment in granulites: experimental phase diagram at 5–7 kbar, 900°C and wetting textures. *Eur. J. Mineral.* 10:1109–23

Guo X, Yoshino T, Shimojuku A. 2015. Electrical conductivity of albite–(quartz)–water and albite–water–NaCl systems and its implication to the high conductivity anomalies in the continental crust. *Earth Planet. Sci. Lett.* 412:1–9

Harvey AH, Prausnitz JM. 1987. Dielectric constants of fluid mixtures over a wide range of temperature and density. *J. Solut. Chem.* 16:857–69

Hauzenberger CA, Baumgartner LP, Pak TM. 2001. Experimental study on the solubility of the "model"-pelite mineral assemblage albite + K-feldspar + andalusite + quartz in supercritical chloride-rich aqueous solutions at 0.2 GPa and 600°C. *Geochim. Cosmochim. Acta* 65:4493–507

Hayden LA, Manning CE. 2011. Rutile solubility in supercritical $NaAlSi_3O_8$–H_2O fluids. *Chem. Geol.* 284:74–81

Heinrich W. 2007. Fluid immiscibility in metamorphic rocks. *Rev. Mineral. Geochem.* 65:389–430

Helgeson HC. 1969. Thermodynamics of hydrothermal systems at elevated temperatures and pressures. *Am. J. Sci.* 267:729–804

Helgeson HC, Kirkham DH. 1976. Theoretical prediction of the thermodynamic behavior of aqueous electrolytes at high pressures and temperatures: III. Equation of state for aqueous species at infinite dilution. *Am. J. Sci.* 276:97–240

Helgeson HC, Kirkham DH, Flowers GC. 1981. Theoretical prediction of the thermodynamic behavior of aqueous electrolytes at high pressures and temperatures: IV. Calculation of activity coefficients, osmotic coefficients, and apparent molal and standard and relative partial molal properties to 600°C and 5 kb. *Am. J. Sci.* 281:1249–516

Holbrook WS, Mooney WD, Christensen NI. 1992. The seismic velocity structure of the deep continental crust. *Cont. Lower Crust* 23:1–43

Holzapfel WB. 1969. Effect of pressure and temperature on the conductivity and ionic dissociation of water up to 100 kbar and 1000°C. *J. Chem. Phys.* 50:4424–28

Huang W, Wyllie P. 1974. Melting relations of muscovite with quartz and sanidine in the K_2O-Al_2O_3-SiO_2-H_2O system to 30 kilobars and an outline of paragonite melting relations. *Am. J. Sci.* 274:378–95

Hunt JD, Kavner A, Schauble EA, Snyder D, Manning CE. 2011. Polymerization of aqueous silica in H_2O-K_2O solutions at 25–200°C and 1 bar to 20 kbar. *Chem. Geol.* 283:161–70

Hunt JD, Manning CE. 2012. A thermodynamic model for the system SiO_2-H_2O near the upper critical end point based on quartz solubility experiments at 500–1100°C and 5–20 kbar. *Geochim. Cosmochim. Acta* 86:196–213

Hyndman R, Shearer P. 1989. Water in the lower continental crust: modelling magnetotelluric and seismic reflection results. *Geophys. J. Int.* 98:343–65

Ichiki M, Baba K, Toh H, Fuji-ta K. 2009. An overview of electrical conductivity structures of the crust and upper mantle beneath the northwestern Pacific, the Japanese Islands, and continental East Asia. *Gondwana Res.* 16:545–62

Jahn S, Schmidt C. 2010. Speciation in aqueous $MgSO_4$ fluids at high pressures and high temperatures from ab initio molecular dynamics and Raman spectroscopy. *J. Phys. Chem. B* 114:15565–72

Kao H, Shan SJ, Dragert H, Rogers G, Cassidy JF, Ramachandran K. 2005. A wide depth distribution of seismic tremors along the northern Cascadia margin. *Nature* 436:841

Kelemen PB, Manning CE. 2015. Reevaluating carbon fluxes in subduction zones, what goes down, mostly comes up. *PNAS* 112:E3997–4006

Kennedy GC, Wasserburg GJ, Heard HC, Newton RC. 1962. The upper three-phase region in the system SiO_2-H_2O. *Am. J. Sci.* 260:501–21

Lamb WM, Valley JW. 1987. Post-metamorphic CO_2-rich inclusions in granulites. *Contrib. Mineral. Petrol.* 96:485–95

Lamb WM, Valley JW. 1988. Granulite facies amphibole and biotite equilibria, and calculated peak-metamorphic water activities. *Contrib. Mineral. Petrol.* 100:349–60

Laumonier M, Gaillard F, Muir D, Blundy J, Unsworth M. 2017. Giant magmatic water reservoirs at mid-crustal depth inferred from electrical conductivity and the growth of the continental crust. *Earth Planet. Sci. Lett.* 457:173–80

Li S, Unsworth MJ, Booker JR, Wei W, Tan H, Jones AG. 2003. Partial melt or aqueous fluid in the mid-crust of Southern Tibet? Constraints from INDEPTH magnetotelluric data. *Geophys. J. Int.* 153:289–304

Liebscher A. 2010. Aqueous fluids at elevated pressure and temperature. *Geofluids* 10:3–19

Makhluf A, Newton R, Manning C. 2016. Hydrous albite magmas at lower crustal pressure: new results on liquidus H_2O content, solubility, and H_2O activity in the system $NaAlSi_3O_8$–H_2O–NaCl at 1.0 GPa. *Contrib. Mineral. Petrol.* 171:75

Manning CE. 1994. The solubility of quartz in H_2O in the lower crust and upper mantle. *Geochim. Cosmochim. Acta* 58:4831–39

Manning CE. 1998. Fluid composition at the blueschist-eclogite transition in the model system Na_2O-MgO-Al_2O_3-SiO_2-H_2O-HCl. *Schweiz. Mineral. Petrogr. Mitt.* 78:225–42

Manning CE. 2004. The chemistry of subduction-zone fluids. *Earth Planet. Sci. Lett.* 223:1–16

Manning CE. 2007. Solubility of corundum plus kyanite in H_2O at 700°C and 10 kbar: evidence for Al-Si complexing at high pressure and temperature. *Geofluids* 7:258–69

Manning CE. 2013. Thermodynamic modeling of fluid-rock interaction at conditions of the Earth's middle crust to upper mantle. *Rev. Mineral. Geochem.* 76:135–64

Manning CE. 2017. The influence of pressure on the properties and origins of hydrous silicate melts in Earth's interior. In *Magmas Under Pressure: Advances in High-Pressure Experiments on Structure and Properties of Melts*, ed. Y Kono, C Sanloup. Amsterdam: Elsevier. In press

Manning CE, Antignano A, Lin HA. 2010. Premelting polymerization of crustal and mantle fluids, as indicated by the solubility of albite + paragonite + quartz in H_2O at 1 GPa and 350–620°C. *Earth Planet. Sci. Lett.* 292:325–36

Manning CE, Aranovich LY. 2014. Brines at high pressure and temperature: thermodynamic, petrologic and geochemical effects. *Precambrian Res.* 253:6–16

Manning CE, Ingebritsen S. 1999. Permeability of the continental crust: implications of geothermal data and metamorphic systems. *Rev. Geophys.* 37:127–50

Manning CE, Shock EL, Sverjensky DA. 2013. The chemistry of carbon in aqueous fluids at crustal and upper-mantle conditions: experimental and theoretical constraints. *Rev. Mineral. Geochem.* 75:109–48

Mantegazzi D, Sanchez-Valle C, Driesner T. 2013. Thermodynamic properties of aqueous NaCl solutions to 1073 K and 4.5 GPa, and implications for dehydration reactions in subducting slabs. *Geochim. Cosmochim. Acta* 121:263–90

Mao S, Hu J, Zhang Y, Lü M. 2015. A predictive model for the *PVTx* properties of CO_2–H_2O–NaCl fluid mixture up to high temperature and high pressure. *Appl. Geochem.* 54:54–64

Markl G, Bucher K. 1998. Composition of fluids in the lower crust inferred from metamorphic salt in lower crustal rocks. *Nature* 391:781–83

Marshall WL, Franck EU. 1981. Ion product of water substance, 0–1000°C, 1–10,000 bars: new international formulation and its background. *J. Phys. Chem. Ref. Data* 10:295–304

McGary RS, Evans RL, Wannamaker PE, Elsenbeck J, Rondenay S. 2014. Pathway from subducting slab to surface for melt and fluids beneath Mount Rainier. *Nature* 511:338–40

Meqbel NM, Egbert GD, Wannamaker PE, Kelbert A, Schultz A. 2014. Deep electrical resistivity structure of the northwestern US derived from 3-D inversion of USArray magnetotelluric data. *Earth Planet. Sci. Lett.* 402:290–304

Mishina M. 2009. Distribution of crustal fluids in Northeast Japan as inferred from resistivity surveys. *Gondwana Res.* 16:563–71

Mookherjee M, Keppler H, Manning CE. 2014. Aluminum speciation in aqueous fluids at deep crustal pressure and temperature. *Geochim. Cosmochim. Acta* 133:128–41

Mountain RD, Harvey AH. 2015. Molecular dynamics evaluation of dielectric constant mixing rules for H_2O–CO_2 at geologic conditions. *J. Solut. Chem.* 44:2179–93

Mysen BO. 2010. Speciation and mixing behavior of silica-saturated aqueous fluid at high temperature and pressure. *Am. Mineral.* 95:1807–16

Nesbitt BE. 1993. Electrical resistivities of crustal fluids. *J. Geophys. Res.* 98:4301–10

Newton RC. 1980. Late Archaean/Early Proterozoic CO_2 streaming through the lower crust and geochemical segregation. *Geophys. Res. Lett.* 14:287–90

Newton RC, Aranovich LY, Hansen EC, Vandenheuvel BA. 1998. Hypersaline fluids in Precambrian deep-crustal metamorphism. *Precambrian Res.* 91:41–63

Newton RC, Manning CE. 2000. Quartz solubility in H_2O-NaCl and H_2O-CO_2 solutions at deep crust-upper mantle pressures and temperatures: 2–15 kbar and 500–900°C. *Geochim. Cosmochim. Acta* 64:2993–3005

Newton RC, Manning CE. 2002a. Experimental determination of calcite solubility in H_2O-NaCl solutions at deep crust/upper mantle pressures and temperatures: implications for metasomatic processes in shear zones. *Am. Mineral.* 87:1401–9

Newton RC, Manning CE. 2002b. Solubility of silica in equilibrium with enstatite, forsterite, and H_2O at deep crust/upper mantle pressures and temperatures and an activity-concentration model for polymerization of aqueous silica. *Geochim. Cosmochim. Acta* 66:4165–76

Newton RC, Manning CE. 2003. Activity coefficient and polymerization of aqueous silica at 800°C, 12 kbar, from solubility measurements on SiO_2-buffering mineral assemblages. *Contrib. Mineral. Petrol.* 146:135–43

Newton RC, Manning CE. 2006. Solubilities of corundum, wollastonite and quartz in H_2O-NaCl solutions at 800°C and 10 kbar: interaction of simple minerals with brines at high pressure and temperature. *Geochim. Cosmochim. Acta* 70:5571–82

Newton RC, Manning CE. 2007. Solubility of grossular, $Ca_3Al_2Si_3O_{12}$, in H_2O-NaCl solutions at 800°C and 10 kbar, and the stability of garnet in the system $CaSiO_3$-Al_2O_3-H_2O-NaCl. *Geochim. Cosmochim. Acta* 71:5191–202

Newton RC, Manning CE. 2008a. Solubility of corundum in the system Al_2O_3-SiO_2-H_2O-NaCl at 800°C and 10 kbar. *Chem. Geol.* 249:250–61

Newton RC, Manning CE. 2008b. Thermodynamics of SiO_2-H_2O fluid near the upper critical end point from quartz solubility measurements at 10 kbar. *Earth Planet. Sci. Lett.* 274:241–49

Newton RC, Manning CE. 2009. Hydration state and activity of aqueous silica in H_2O-CO_2 fluids at high pressure and temperature. *Am. Mineral.* 94:1287–90

Newton RC, Manning CE. 2010. Role of saline fluids in deep-crustal and upper-mantle metasomatism: insights from experimental studies. *Geofluids* 10:58–72

Newton RC, Manning CE. 2016. Evidence for SiO_2-NaCl complexing in H_2O-NaCl solutions at high pressure and temperature. *Geofluids* 16:342–48

Newton RC, Smith JV, Windley BF. 1980. Carbonic metamorphism, granulites and crustal growth. *Nature* 288:45–50

Newton RC, Touret JL, Aranovich LY. 2014. Fluids and H_2O activity at the onset of granulite facies metamorphism. *Precambrian Res.* 253:17–25

Ogawa Y, Mishina M, Goto T, Satoh H, Oshiman N, et al. 2001. Magnetotelluric imaging of fluids in intraplate earthquake zones, NE Japan back arc. *Geophys. Res. Lett.* 28:3741–44

Pan D, Galli G. 2016. The fate of carbon dioxide in water-rich fluids at extreme conditions. *Sci. Adv.* 2:e1601278

Pan D, Spanu L, Harrison B, Sverjensky DA, Galli G. 2013. The dielectric properties of water under extreme conditions and transport of carbonates in the deep Earth. *PNAS* 110:6646–50

Pan D, Wan Q, Galli G. 2014. The refractive index and electronic gap of water and ice increase with increasing pressure. *Nat. Commun.* 5:3919

Pokrovski GS, Dubrovinsky LS. 2011. The S_3^- ion is stable in geological fluids at elevated temperatures and pressures. *Science* 331:1052–54

Quist AS, Marshall WL. 1968. Electrical conductances of aqueous sodium chloride solutions from 0 to 800° and pressures to 4000 bars. *J. Phys. Chem.* 68:684–703

Quist AS, Marshall WL. 1969. Electrical conductances of some alkali metal halides in aqueous solutions from 0 to 800° and at pressures to 4000 bars. *J. Phys. Chem.* 73:978–85

Reyners M, Eberhart-Phillips D. 2009. Small earthquakes provide insight into plate coupling and fluid distribution in the Hikurangi subduction zone, New Zealand. *Earth Planet. Sci. Lett.* 282:299–305

Rudnick R, Gao S. 2003. Composition of the continental crust. In *Treatise on Geochemistry*, Vol. 3: *The Crust*, ed. HD Holland, KK Turekian, pp. 1–64. Oxford, UK: Elsevier. 1st ed.

Sahle CJ, Sternemann C, Schmidt C, Lehtola S, Jahn S, et al. 2013. Microscopic structure of water at elevated pressures and temperatures. *PNAS* 110:6301–6

Sakuma H, Ichiki M. 2016a. Density and isothermal compressibility of supercritical H_2O-NaCl fluid: molecular dynamics study from 673 to 2000 K, 0.2 to 2 GPa, and 0 to 22 wt% NaCl concentrations. *Geofluids* 16:89–102

Sakuma H, Ichiki M. 2016b. Electrical conductivity of NaCl-H_2O fluid in the crust. *J. Geophys. Res.* 121:577–94

Sakuma H, Ichiki M, Kawamura K, Fuji-ta K. 2013. Prediction of physical properties of water under extremely supercritical conditions: a molecular dynamics study. *J. Chem. Phys.* 138:134506

Sanchez-Valle C. 2013. Structure and thermodynamics of subduction zone fluids from spectroscopic studies. *Rev. Mineral. Geochem.* 76:265–309

Sanchez-Valle C, Mantegazzi D, Bass JD, Reusser E. 2013. Equation of state, refractive index and polarizability of compressed water to 7 GPa and 673 K. *J. Chem. Phys.* 138:054505

Schmidt C. 2014. Raman spectroscopic determination of carbon speciation and quartz solubility in H_2O + Na_2CO_3 and H_2O + $NaHCO_3$ fluids to 600°C and 1.53 GPa. *Geochim. Cosmochim. Acta* 145:281–96

Schmidt C, Chou IM. 2012. The hydrothermal diamond anvil cell (HDAC) for Raman spectroscopic studies of geological fluids at high pressures and temperatures. In *Applications of Raman Spectroscopy to Earth Sciences and Cultural Heritage*, ed. J Dubessy, MC Caumon, F Rull, pp. 249–78. Eur. Mineral. U. Notes Mineral. 12. Chantilly, VA: Mineral. Soc. Am.

Schmidt C, Manning CE. 2017. Pressure-induced ion pairing in $MgSO_4$ solutions: implications for the oceans of icy worlds. *Geochem. Perspect. Lett.* 3:66–74

Shankland TJ, Ander ME. 1983. Electrical conductivities, temperatures, and fluids in the lower crust. *J. Geophys. Res.* 88:9475–84

Shaw DM. 1956. Geochemistry of pelitic rocks. Part III: Major elements and general geochemistry. *Geol. Soc. Am. Bull.* 67:919–34

Shelly DR, Hardebeck JL. 2010. Precise tremor source locations and amplitude variations along the lower-crustal central San Andreas fault. *Geophys. Res. Lett.* 37:L14301

Shen A, Keppler H. 1997. Direct observation of complete miscibility in the albite-H_2O system. *Nature* 385:710–12

Shimojuku A, Yoshino T, Yamazaki D. 2014. Electrical conductivity of brine-bearing quartzite at 1 GPa: implications for fluid content and salinity of the crust. *Earth Planets Space* 66:2

Shimojuku A, Yoshino T, Yamazaki D, Okudaira T. 2012. Electrical conductivity of fluid-bearing quartzite under lower crustal conditions. *Phys. Earth Planet. Inter.* 198:1–8

Shmulovich K, Graham C, Yardley BWD. 2001. Quartz, albite and diopside solubilities in H_2O-NaCl and H_2O-CO_2 fluids at 0.5–0.9 GPa. *Contrib. Mineral. Petrol.* 141:95–108

Shmulovich KI, Yardley BWD, Graham CM. 2006. Solubility of quartz in crustal fluids: experiments and general equations for salt solutions and H_2O–CO_2 mixtures at 400–800°C and 0.1–0.9 GPa. *Geofluids* 6:154–67

Sinmyo R, Keppler H. 2017. Electrical conductivity of NaCl-bearing aqueous fluids to 600°C and 1 GPa. *Contrib. Mineral. Petrol.* 172:4

Skelton A, Valley J, Graham C, Bickle M, Fallick A. 2000. The correlation of reaction and isotope fronts and the mechanism of metamorphic fluid flow. *Contrib. Mineral. Petrol.* 138:364–75

Sverjensky DA, Harrison B, Azzolini D. 2014. Water in the deep Earth: the dielectric constant and the solubilities of quartz and corundum to 60 kb and 1200°C. *Geochim. Cosmochim. Acta* 129:125–45

Tanger JC IV, Helgeson HC. 1988. Calculation of the thermodynamic and transport properties of aqueous species at high pressures and temperatures: revised equations of state for the standard partial molal properties of ions and electrolytes. *Am. J. Sci.* 288:19–98

Thompson AB, Connolly JAD. 1990. Metamorphic fluids and anomalous porosities in the lower crust. Tectonophysics 182:47–55

Touret JLR. 1985. Fluid regime in southern Norway: the record of fluid inclusions. In *The Deep Proterozoic Crust in the North Atlantic Provinces*, ed. AC Tobi, JLR Touret, pp. 517–49. Dordrecht, Neth.: Reidel

Touret JLR. 2001. Fluids in metamorphic rocks. *Lithos* 55:1–25

Trommsdorff V, Skippen G, Ulmer P. 1985. Halite and sylvite as solid inclusions in high-grade metamorphic rocks. *Contrib. Mineral. Petrol.* 89:24–29

Tropper P, Manning CE. 2005. Very low solubility of rutile in H_2O at high pressure and temperature, and its implications for Ti mobility in subduction zones. *Am. Mineral.* 90:502–5

Tropper P, Manning CE. 2007. The solubility of corundum in H_2O at high pressure and temperature and its implications for Al mobility in the deep crust and upper mantle. *Chem. Geol.* 240:54–60

Waff HS. 1974. Theoretical considerations of electrical conductivity in a partially molten mantle and implications for geothermometry. *J. Geophys. Res.* 79:4003–10

Walrafen G, Yang WH, Chu Y, Hokmabadi M. 1996. Raman OD-stretching overtone spectra from liquid D_2O between 22 and 152°C. *J. Phys. Chem.* 100:1381–91

Walther JV, Orville PM. 1983. The extraction-quench technique for determination of the thermodynamic properties of solute complexes: application to quartz solubility in fluid mixtures. *Am. Mineral.* 68:731–41

Wannamaker PE. 2000. Comment on "The petrologic case for a dry lower crust" by Bruce W.D. Yardley and John W. Valley. *J. Geophys. Res.* 105:6057–64

Wannamaker PE, Evans RL, Bedrosian PA, Unsworth MJ, Maris V, McGary RS. 2014. Segmentation of plate coupling, fate of subduction fluids, and modes of arc magmatism in Cascadia, inferred from magnetotelluric resistivity. *Geochem. Geophys. Geosyst.* 15:4230–53

Wannamaker PE, Jiracek GR, Stodt JA, Caldwell TG, Gonzalez VM, et al. 2002. Fluid generation and pathways beneath an active compressional orogen, the New Zealand Southern Alps, inferred from magnetotelluric data. *J. Geophys. Res.* 107:ETG6-1–ETG6-20

Wei W, Unsworth M, Jones A, Booker J, Tan H, et al. 2001. Detection of widespread fluids in the Tibetan crust by magnetotelluric studies. *Science* 292:716–19

Wolery TJ. 1992. *EQ3/6, a software package for geochemical modeling of aqueous systems: package overview and installation guide (Version 7.0)*. Rep. UCRL-MA–110662-PT.1, Lawrence Livermore Natl. Lab., Livermore, CA

Worzewski T, Jegen M, Kopp H, Brasse H, Castillo WT. 2011. Magnetotelluric image of the fluid cycle in the Costa Rican subduction zone. *Nat. Geosci.* 4:108

Xie Z, Walther JV. 1993. Quartz solubilities in NaCl solutions with and without wollastonite at elevated temperatures and pressures. *Geochim. Cosmochim. Acta* 57:1947–55

Yardley BWD, Bodnar RJ. 2014. Fluids in the continental crust. *Geochem. Perspect.* 3:1–2

Yardley BWD, Bottrell SH. 1992. Silica mobility and fluid movement during metamorphism of the Connemara schists, Ireland. *J. Metamorph. Geol.* 10:453–64

Yardley BWD, Bottrell SH, Cliff RA. 1991. Evidence for a regional-scale fluid loss event during mid-crustal metamorphism. *Nature* 349:151–54

Yardley BWD, Graham JT. 2002. The origins of salinity in metamorphic fluids. *Geofluids* 2:249–56

Yardley BWD, Valley JW. 1997. The petrologic case for a dry lower crust. *J. Geophys. Res.* 102:12173–85
Yoshii N, Miura S, Okazaki S. 2001. A molecular dynamics study of dielectric constant of water from ambient to sub- and supercritical conditions using a fluctuating-charge potential model. *Chem. Phys. Lett.* 345:195–200
Zhang YG, Frantz JD. 2000. Enstatite-forsterite-water equilibria at elevated temperatures and pressures. *Am. Mineral.* 85:918–25
Zhang Z, Duan Z. 2005. Prediction of the *PVT* properties of water over wide range of temperatures and pressures from molecular dynamics simulation. *Phys. Earth Planet. Inter.* 149:335
Zhao D, Kanamori H, Negishi H, Wiens D. 1996. Tomography of the source area of the 1995 Kobe earthquake: evidence for fluids at the hypocenter? *Science* 274:1891–94
Zhao D, Mishra O, Sanda R. 2002. Influence of fluids and magma on earthquakes: seismological evidence. *Phys. Earth Planet. Inter.* 132:249–67
Zotov N, Keppler H. 2000. In-situ Raman spectra of dissolved silica species in aqueous fluids to 900°C and 14 kbar. *Am. Mineral.* 85:600–4
Zotov N, Keppler H. 2002. Silica speciation in aqueous fluids at high pressures and high temperatures. *Chem. Geol.* 184:71–82

Annual Review
of Earth and
Planetary Sciences
Volume 46, 2018

Contents

Errata

An online log of corrections to *Annual Review of Earth and Planetary Sciences* articles may be found at http://www.annualreviews.org/errata/earth